Cell

Article

Quiescent cell re-entry is limited by macroautophagy-induced lysosomal damage

Graphical abstract

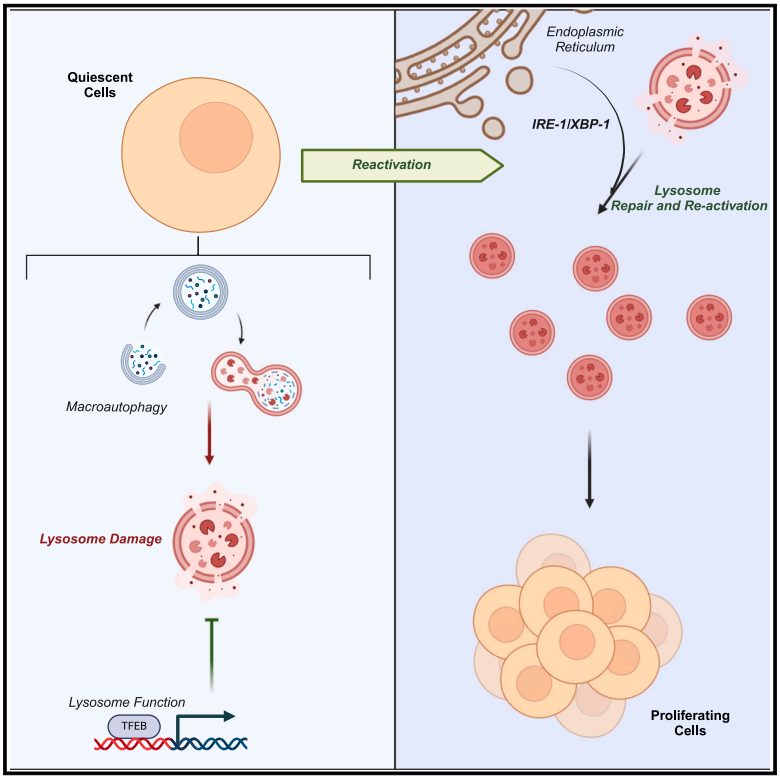

Highlights

- Intra-lysosomal protein aggregates accumulate via autophagy in quiescent cells
- Lysosomes are damaged via autophagy in quiescent cells
- Inhibiting autophagy and increasing lysosome activity synergize to reduce damage
- IRE-1/XBP-1 promote repair of damaged lysosomes and quiescent cell reactivation

Authors

Andrew Murley, Ann Catherine Popovici, Xiwen Sophie Hu, ..., Hanlin Zhang, Naomi R. Genuth, Andrew Dillin

Correspondence

dillin@berkeley.edu

In brief

Lysosomes are damaged in quiescent cells, and UPR regulators, IRE-1/XBP-1, promote lysosome repair for cell-cycle re-entry. Lysosome damage in quiescent cells is caused in part by macroautophagy and is suppressed in a synergistic way by inhibiting macroautophagy and boosting lysosome activity.

Murley et al., 2025, Cell *188*, 1–17
May 15, 2025
https://doi.org/10.1016/j.cell.2025.03.009

CellPress

Please cite this article in press as: Murley et al., Quiescent cell re-entry is limited by macroautophagy-induced lysosomal damage, Cell (2025), https://doi.org/10.1016/j.cell.2025.03.009

Cell

CellPress

Article

Quiescent cell re-entry is limited by macroautophagy-induced lysosomal damage

Andrew Murley,[1] Ann Catherine Popovici,[1] Xiwen Sophie Hu,[1] Anina Lund,[1] Kevin Wickham,[1] Jenni Durieux,[1] Larry Joe,[1] Etai Koronyo,[1] Hanlin Zhang,[1] Naomi R. Genuth,[1] and Andrew Dillin[1,2,3,*]

[1]Department of Molecular and Cell Biology, University of California, Berkeley, Berkeley, CA, USA
[2]Howard Hughes Medical Institute, University of California, Berkeley, Berkeley, CA, USA
[3]Lead contact
*Correspondence: dillin@berkeley.edu
https://doi.org/10.1016/j.cell.2025.03.009

SUMMARY

To maintain tissue homeostasis, many cells reside in a quiescent state until prompted to divide. The reactivation of quiescent cells is perturbed with aging and may underlie declining tissue homeostasis and resiliency. The unfolded protein response regulators IRE-1 and XBP-1 are required for the reactivation of quiescent cells in developmentally L1-arrested *C. elegans*. Utilizing a forward genetic screen in *C. elegans*, we discovered that macroautophagy targets protein aggregates to lysosomes in quiescent cells, leading to lysosome damage. Genetic inhibition of macroautophagy and stimulation of lysosomes via the overexpression of HLH-30 (TFEB/TFE3) synergistically reduces lysosome damage. Damaged lysosomes require IRE-1/XBP-1 for their repair following prolonged L1 arrest. Protein aggregates are also targeted to lysosomes by macroautophagy in quiescent cultured mammalian cells and are associated with lysosome damage. Thus, lysosome damage is a hallmark of quiescent cells, and limiting lysosome damage by restraining macroautophagy can stimulate their reactivation.

INTRODUCTION

Age is associated with declining tissue function and diminished capacity for repair.[1] Adult somatic stem cells, such as hematopoietic stem cells, neural stem cells, and muscle stem cells, give rise to new cell types within blood, brain, and muscle tissues, respectively.[2,3] These adult stem cells divide infrequently, mainly residing in a quiescent (G_0) cell state until called upon to proliferate in response to specific conditions.[3] Quiescence is a general regulator of tissue and organismal homeostasis and is an important feature of other cells in the body, including lymphocytes and hepatocytes.[2] Studies in model organisms and humans indicate that aging and age-associated diseases compromise the reactivation of quiescent cells, which may contribute to tissue dysfunction with age.[4–8] The mechanisms leading to adult stem cell dysfunction with age are incompletely understood but are influenced by cell-intrinsic properties and signals from their niche.[3,4] Identifying processes that contribute to the age-associated decline in stem cell function may identify ways to harness the body's innate capacity for repair and rejuvenation throughout life.

Quiescence is a mechanism that eukaryotic cells employ in response to conditions that are not conducive to growth, either to maintain tissue homeostasis or because essential nutrients are limiting. In single-celled eukaryotes and less-complex animals such as *C. elegans*, one of the main signals inducing cellular quiescence is nutrient deprivation. When born without food, *C. elegans* L1 larvae arrest their development until they encounter sufficient food sources, termed L1 arrest. At the cellular level, during L1 arrest, reduced insulin-like growth factor (IGF) signaling activates the transcription factor DAF-16 (FOXO), inducing transcriptional upregulation of the cyclin-dependent kinase inhibitor CKI-1/2 (p21/p27), which arrests the post-embryonic division of cells.[9–11] *C. elegans* can survive L1 arrest for a few weeks; however, over time, animals lose the ability to develop into adults, remaining permanently arrested as L1 larvae.[12] Cellular integrity influences the ability of animals to recover from prolonged L1 arrest, with animals that accumulate more reactive-oxygen species (ROS), protein aggregates, and fragmented mitochondria over time being unable to re-enter development.[12] These signs of cellular dysfunction resemble those found in aging, suggesting the mechanisms leading to permanent arrest of *C. elegans* L1 larvae may be similar to those restricting the reactivation of quiescent cells in aged mammals, such as adult somatic stem cells.

Numerous homeostatic mechanisms maintain the function of quiescent cells. Being mitotically arrested, quiescent cells generally have lower anabolic rates, which is maintained in part by reduced mechanistic target-of-rapamycin (mTOR) activity.[13–15] Reduced mTOR signaling in quiescent cells helps to inhibit their growth and transition to cellular senescence, which is characterized by high mTOR signaling that is resistant to

Please cite this article in press as: Murley et al., Quiescent cell re-entry is limited by macroautophagy-induced lysosomal damage, Cell (2025), https://doi.org/10.1016/j.cell.2025.03.009

changes in nutrient levels.[16] Aging compromises the autophagy/lysosomal pathways, and various means of counteracting this decline, mainly through stimulation of the transcription factor EB (TFEB), improve quiescent cell homeostasis and reactivation efficiency.[5–7] The unfolded protein response (UPR) of the endoplasmic reticulum (ER) also plays a role in quiescent cell homeostasis. The UPR promotes homeostasis of the ER and responds to increased cellular need for the ER by activating the inositol-requiring enzyme 1 (IRE-1)/X-box binding protein 1 (XBP-1), activating transcription factor 6 (ATF6), and protein kinase R-like endoplasmic reticulum kinase (PERK) pathways, reviewed extensively elsewhere.[17–21] Activation of the UPR is diminished in certain tissues during aging, and previous studies have reported that IRE-1 is required for the development of *C. elegans* after prolonged periods of L1 arrest and that Ire1α is crucial for liver regenerative responses in mice, indicating that diminished quiescent cell reactivation with aging might be influenced by aberrant UPR signaling.[12,22]

In this study, we report that damage to lysosomes is a conserved feature of quiescent cells and compromises their reactivation in the absence of IRE-1 or XBP-1. Macroautophagy makes an important contribution to this damage through the targeting of protein aggregates to lysosomes and, conversely, boosting lysosome biogenesis and inhibiting macroautophagy work synergistically to improve the reactivation of quiescent cells. Because quiescent cell reactivation declines with age, our results suggest that, rather than boosting macroautophagy, one strategy to combat this age-associated decline could be to boost lysosome function while restraining macroautophagy.

RESULTS

Loss-of-function mutations in core macroautophagy genes improve recovery of animals from L1 arrest

Consistent with previous studies, we found that *C. elegans* survived L1 arrest for a few weeks but, over time, lost the ability to develop once fed, which was accelerated in *ire-1* and *xbp-1* mutants (Figures 1A and 1B).[12] Consistent with previous observations, *atf-6* and *pek-1* mutations did not affect recovery from L1 arrest (Figure 1B).[12] The phenotype of *ire-1* and *xbp-1* mutants was also distinct from *hlh-30* mutants, encoding the *C. elegans* ortholog of TFEB, which died rapidly during L1 arrest (Figure 1B). The ability of *ire-1* and *xbp-1* mutants to survive arrest but over time lose the ability to escape it is similar to observations made in a variety of adult stem cells and other quiescent cells in vertebrates whose ability to escape quiescence declines with aging and disease.[4–6,8,23] This phenotype, which is present in wild-type (WT) animals but exacerbated in *ire-1* and *xbp-1* mutants, we term "progressive terminal L1 arrest" or PTLA. In *ire-1* mutants, PTLA correlated with a persistence of seam cells expressing GFP from the *cki-1* promoter, a cell type that becomes arrested during L1 arrest, indicating that UPR dysfunction prevents replication-competent cells in the animals from re-entering the cell cycle (Figures 1C and 1D).[10]

Interestingly, despite being able to eat after prolonged L1 arrest, *ire-1* and *xbp-1* mutants cannot reactivate mTOR complex 1 (mTORC1) signaling, as assessed by phosphorylation of RSKS-1, the *C. elegans* S6 kinase (Figures 1E, 1F, S1A, and S1B).[24,25] As a major sensor of nutrients and growth factors, mTORC1 is a kinase that is active in conditions permissive to cell growth, phosphorylating and activating proteins promoting cell growth, including those involved in protein translation and ribosome biogenesis, and inhibiting catabolic processes such as autophagy.[26] We also assessed activity of nutrient-sensing or growth-regulating pathways, specifically AMPK and ERK. We did not observe significant differences between WT and *ire-1/xbp-1* mutants at later time points of L1 arrest of either pathway, indicating that they are not correlated with PTLA (Figure S1B). Furthermore, although quiescent seam cells remained arrested in *ire-1* mutants fed after prolonged L1 arrest, there was still a significant decrease in GFP expression from *cki-1p::GFP* (Figure 1D). As this reporter is regulated by the transcription factor DAF-16, functioning downstream of growth factor/Akt signaling, this further suggests that growth factor regulation is not defective.[10] Thus, reduced mTORC1 activation and seam cell proliferation in *ire-1/xbp-1* mutants correlated with their inability to develop after prolonged L1 arrest.

To identify mechanisms leading to PTLA in *ire-1* mutants, we conducted a forward genetic screen for mutations that would bypass the requirement for IRE-1 in L1 arrest. We isolated F2 progeny from ethyl methanesulfonate (EMS)-mutagenized *ire-1(ok799)* and *ire-1(zc14)* animals and L1 arrested them for a period during which all *ire-1* mutants lose the ability to develop, but WT animals remain capable of developing. After L1 arrest, we allowed animals to recover on plates with food. Animals that reached adulthood and were fertile were used to establish lines that were re-tested, then subjected to whole-genome sequencing to identify candidate mutations (Figure 2A).

Among the genes identified in our screen were, surprisingly, strong loss-of-function alleles in macroautophagy genes (Figure 2B). Macroautophagy (herein "autophagy") is an ancient mechanism that eukaryotic cells employ to engulf superfluous, damaged, or toxic cellular components in double-membrane structures called autophagosomes, which fuse with lysosomes that degrade autophagosome cargo.[27] We isolated lines with three independent mutations in *atg-9*, two resulting in premature stop codons (*atg-9(Q428Stop)* and *atg-9(W642Stop)*) and one in a highly conserved proline residue that, based on structural homology, likely generates a loss-of-function allele (*atg-9(P495S)*) (Figure 2B). ATG-9 is the sole transmembrane protein in the core autophagic machinery and forms a homotrimeric complex that functions as a phospholipid scramblase.[28–31] *atg-9* is the sole homolog of yeast *ATG9* in *C. elegans*. We also isolated a premature stop codon in one of two *C. elegans* homologs of yeast *ATG4*, *atg-4.1* (*atg-4.1(N156Stop)*) (Figure 2B). Akin to yeast Atg4, ATG-4.1 is a cysteine peptidase that is required for processing of LGG-1 (Atg8/LC3), the core component of autophagic membranes. In *C. elegans*, ATG-4.1 and its paralog ATG-4.2 have somewhat overlapping functions in autophagy, and double *atg-4.1;atg-4.2* mutants are not viable.[32,33] Other mutations we identified in *atg*-3 (involved in lipidation of LGG-1) and *atg-18* are predicted to be detrimental to the function of the proteins encoded by those genes (Figure 2B). Notably, all the proteins encoded by these genes function early in autophagy, i.e., in autophagosome formation but not in lysosomal fusion of autophagosomes or lysosomal degradation processes.

Please cite this article in press as: Murley et al., Quiescent cell re-entry is limited by macroautophagy-induced lysosomal damage, Cell (2025), https://doi.org/10.1016/j.cell.2025.03.009

CellPress

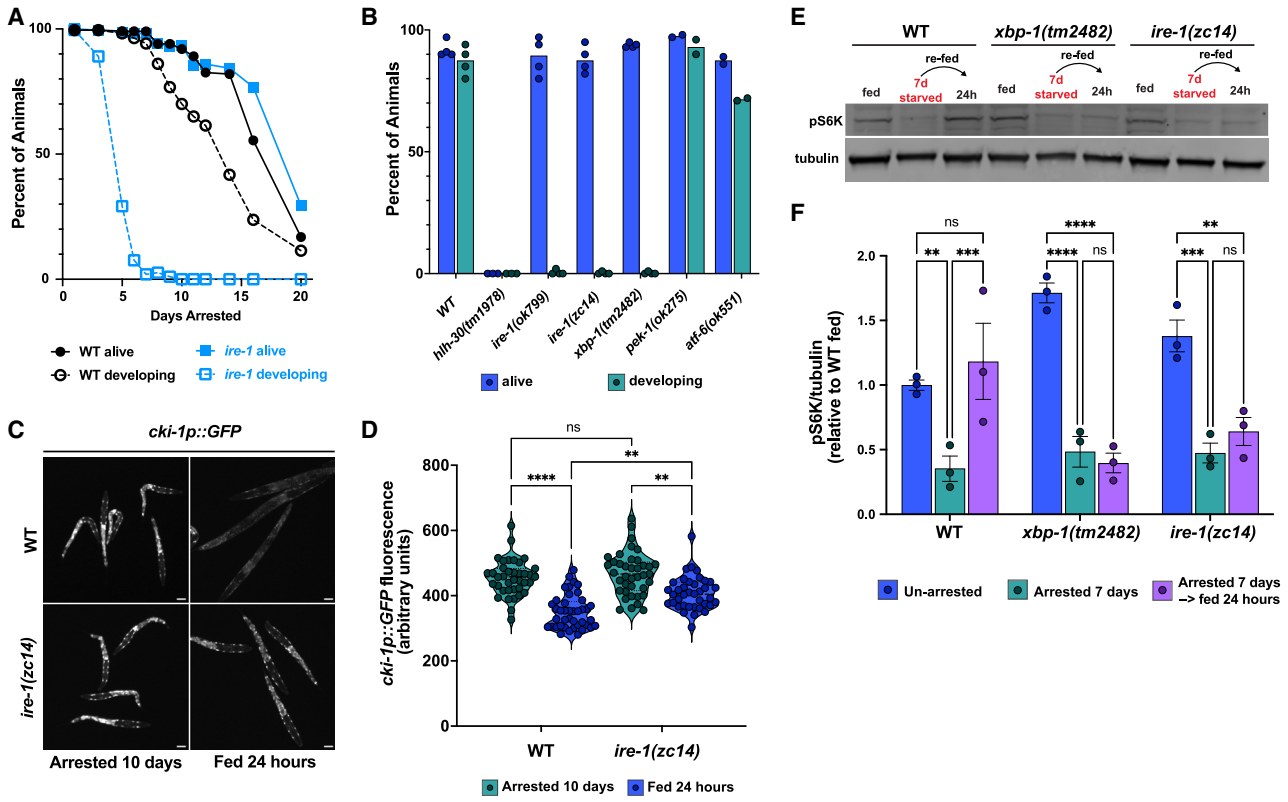

Figure 1. IRE-1 and XBP-1 are required for the reactivation of mTORC1 after prolonged L1 arrest

(A) WT and *ire-1(zc14)* were L1 arrested, and every other day, animals were given food and immediately scored for viability and development as described in STAR Methods.

(B) Animals of the indicated genotypes were subjected to L1 arrest for 10 days, then given food and assessed for viability and development as described in STAR Methods.

(C) WT and *ire-1(zc14)* animals expressing GFP driven by the CKI-1 promoter (*cki-1p::GFP*) were L1 arrested for 10 days and then fed for 24 h and imaged. Scale bars, 20 μm.

(D) Quantification of GFP fluorescence in *cki-1p::GFP* animals L1 arrested for 10 days and fed for 24 h. *p* values calculated using Kruskal-Wallis test followed by a post hoc analysis using Dunn's multiple comparisons test. $^{*}p < 0.05$, $^{**}p < 0.01$, $^{***}p < 0.001$, $^{****}p < 0.0001$, ns, no significance.

(E) Representative western blot of pS6K and α-tubulin in WT, *xbp-1(tm2482)*, and *ire-1(zc14)* L1 larvae that were fed (un-arrested), animals L1 arrested for 7 days (7d starved), and animals L1 arrested for 7 days then fed for 24 h were harvested as described in "STAR Methods" and subjected to western blot analysis.

(F) Quantification and statistical analysis of $n = 3$ biological replicates of pS6K levels relative to tubulin in WT, *xbp-1(tm2482)*, and *ire-1(zc14)* that were un-arrested, arrested for 7 days, or arrested for 7 days then fed for 24 h. Error bars represent standard error of the mean. *p* values calculated using Tukey's post hoc analysis of a two-way ANOVA. $^{*}p < 0.05$, $^{**}p < 0.01$, $^{***}p < 0.001$, $^{****}p < 0.0001$, ns, no significance.

See also Figure S1.

We were surprised to identify such strong hits in core autophagy machinery in our screen because L1 arrest is a starvation response that is thought to require autophagy for organismal survival.[34] To confirm these results, we crossed *ire-1* animals to independently isolated lines harboring null mutations in *atg-9*, *atg-4.1*, and *atg-18*, as well as hypomorphic alleles of the essential genes *atg-3* and *atg-7*, which regulate distinct steps in autophagosome formation, those being *atg-9(bp564), atg-4.1(bp501), atg-18(gk378), atg-3(bp412)*, and *atg-7(bp422)*, respectively.[35] Although *atg-18(gk378)* compromised survival of L1-arrested animals, other mutations improved the recovery of L1-arrested *ire-1(zc14)* mutants after 5 days of arrest, strongly suggesting that autophagy, not other functions of autophagy proteins, is relevant to PTLA (Figures 2C and S2D).[36] In subsequent experiments, described below, we primarily utilized the *atg-9(bp564)* mutation as a model for autophagy inhibition because its growth rate is similar to WT and, unlike *atg-4.1*, it is the only *ATG9* homolog in the *C. elegans* genome. Although mutations in autophagy improved PTLA in *ire-1(zc14)* mutants, they did not fully restore *ire-1(zc14)* mutants to a WT PTLA phenotype, indicating that other processes also influence PTLA (Figure 2D).

Mitochondrial DNA (mtDNA) is degraded by autophagy during L1 arrest, and subsequent mtDNA synthesis and mitochondrial biogenesis via the mitochondrial UPR influence recovery from L1 arrest.[37,38] Given the role the ER plays in mtDNA replication and segregation in cells, IRE-1 and XBP-1 may play a role in mtDNA replication, and, therefore, blocking autophagy may be beneficial by preventing the degradation of mtDNA.[39,40] To test this idea, we asked whether mutations in *pdr-1*, the *C. elegans* ortholog of

Please cite this article in press as: Murley et al., Quiescent cell re-entry is limited by macroautophagy-induced lysosomal damage, Cell (2025), https://doi.org/10.1016/j.cell.2025.03.009

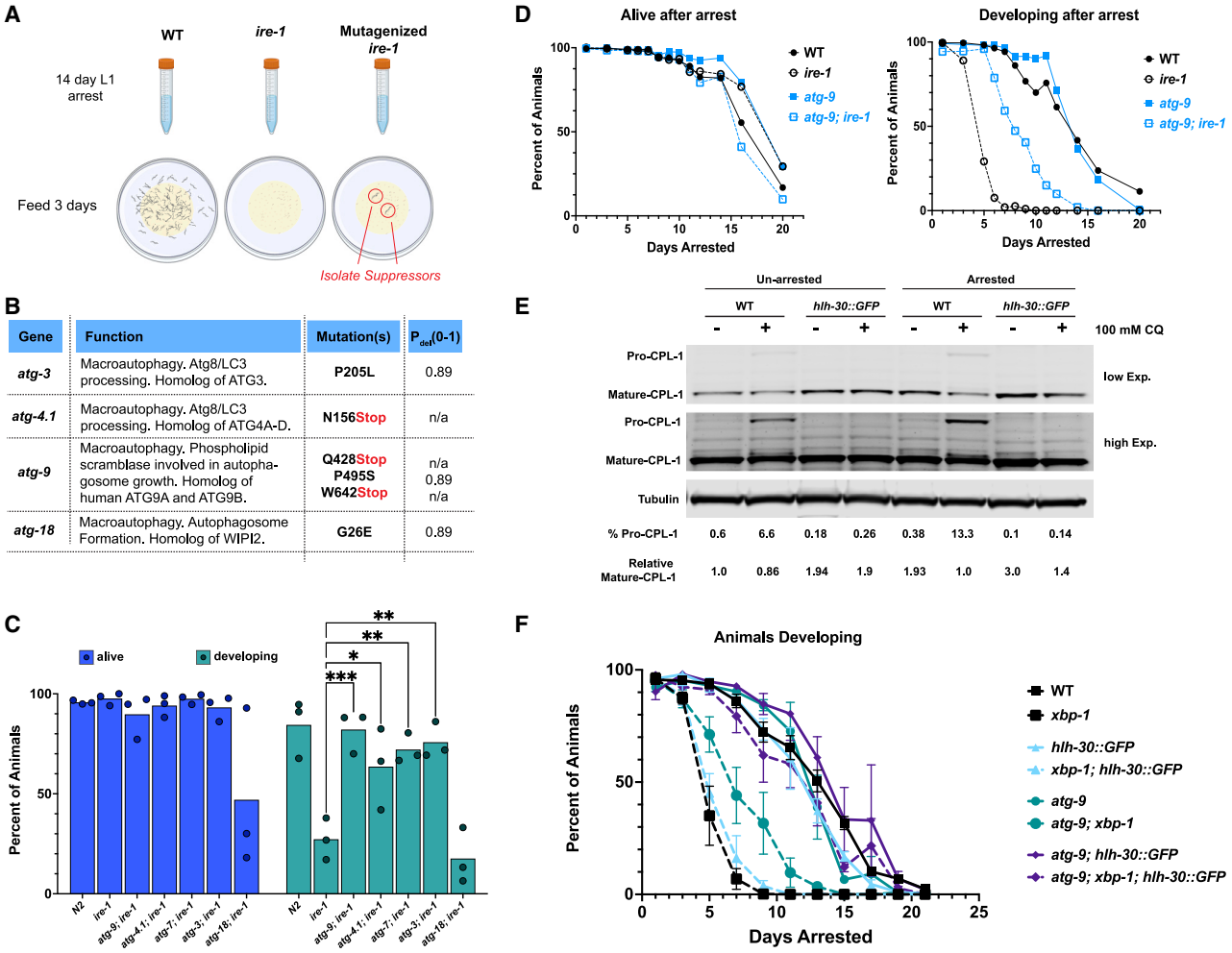

B

Gene	Function	Mutation(s)	P_{del}(0-1)
atg-3	Macroautophagy. Atg8/LC3 processing. Homolog of ATG3.	P205L	0.89
atg-4.1	Macroautophagy. Atg8/LC3 processing. Homolog of ATG4A-D.	N156Stop	n/a
atg-9	Macroautophagy. Phospholipid scramblase involved in autophagosome growth. Homolog of human ATG9A and ATG9B.	Q428Stop P495S W642Stop	n/a 0.89 n/a
atg-18	Macroautophagy. Autophagosome Formation. Homolog of WIPI2.	G26E	0.89

Figure 2. Mutations in core macroautophagy genes synergize with enhanced lysosomal function to promote recovery from L1 arrest

(A) Overview of forward genetic screen for suppressors of PTLA phenotype in *ire-1* mutants, where F2 progeny from EMS-mutagenized *ire-1* mutants were L1 arrested for 14 days, then plated on plates with food. Rare mutants that developed to adulthood and were fertile were used to establish lines that were analyzed by whole-genome sequencing.

(B) Mutations isolated from the screen. "P_{del}" represents the probability the indicated mutation is deleterious to the encoded protein based on protein analysis through evolutionary relationships (PANTHER) protein database. Allele designations for these mutations are listed in the "key resources table" of the STAR Methods section.

(C) Loss-of-function mutations in macroautophagy genes suppresses PTLA. *ire-1(zc14)* mutants were crossed to *atg-3(bp412)*, *atg-4.1(bp501)*, *atg-7(bp422)*, *atg-9(bp564)*, and *atg-18(gk378)* and subjected to a 5-day L1 arrest. *p* values calculated using Dunnett's multiple comparisons test. $^{*}p < 0.05$, $^{**}p < 0.01$, $^{***}p < 0.001$, $^{****}p < 0.0001$, ns, no significance.

(D) *atg-9* mutation suppresses PTLA. Animals of the indicated genotypes were subjected to L1 arrest and periodically assessed for viability and development according to STAR Methods.

(E) Representative western blot of CPL-1 and α-tubulin. Fed (un-arrested) L1 animals and L1 animals arrested for 1 day were treated with 100 mM chloroquine for 1 h. Pro-CPL-1 corresponds to the predicted full-length size of CPL-1, approximately 38 kDa. The low and high exposure blots are included to depict the differing amounts of pro and mature CPL-1.

(F) Reduced autophagy and HLH-30::GFP overexpression synergistically suppress PTLA. Animals of the indicated genotypes were subjected to L1 arrest and periodically assessed for viability and development. Error bars represent standard error of the mean (SEM) for $n = 3$ biological replicates. $^{*}p < 0.05$, $^{**}p < 0.01$, $^{***}p < 0.001$, $^{****}p < 0.0001$, ns, no significance.

See also Figures S2 and S3.

Parkin involved in autophagy of mitochondria (mitophagy), could rescue PTLA in *ire-1* mutants.[41] We found that *pdr-1* mutants had no effect on PTLA in *ire-1* mutants (Figure S2A).

To assess whether blocking autophagy corrects mTORC1 regulation in *ire-1* mutants, we analyzed phosphorylation of RSKS-1 in un-arrested L1 animals, L1 animals arrested for 5 days, and L1 animals arrested for 5 days and fed for 12 h. Consistent with their improved development after L1 arrest, *atg-9; ire-1* mutants also had restored activation of mTORC1 after feeding (Figures S2D–S2F). Consistent with our finding is the

Please cite this article in press as: Murley et al., Quiescent cell re-entry is limited by macroautophagy-induced lysosomal damage, Cell (2025), https://doi.org/10.1016/j.cell.2025.03.009

role of autophagy in regulating the activation of mTORC1 in response to T cell receptor stimulation in Treg cells.[42]

Autophagy inhibition and lysosome biogenesis synergistically improve recovery from L1 arrest

Autophagy is a tightly regulated process in cells, and excessive autophagy can lead to cell death or possibly to the degradation of cellular constituents necessary for cell-cycle re-entry.[43] To test whether increased autophagy is detrimental in *ire-1 or xbp-1* mutants, we overexpressed the *C. elegans* ortholog of *TFE3/TFEB* transcription factors, HLH-30, fused to GFP. These transcription factors boost the autophagic capacity of cells by upregulating genes for lysosome function and autophagosome formation, and consistent with this, overexpression of HLH-30 stimulates autophagic flux in adult *C. elegans*.[44–46] We confirmed that, similar to its effects in adult animals, overexpression of HLH-30::GFP increases expression and processing of the cathepsin L CPL-1, indicating that *hlh-30::GFP* animals have greater lysosomal activity (Figure 2E). Cathepsins are first synthesized in the ER and transported to lysosomes, where they are further cleaved to remove an inhibitory pro-domain to become activated.[47] Thus, amounts of pro-cathepsins and mature cathepsins are a reflection of protein synthesis and trafficking in the secretory pathway and lysosomal activity, respectively.[48] Levels of mature CPL-1 were approximately 2- and 1.5-fold higher in *hlh-30::GFP* L1 animals that were never arrested or arrested for 1 day, respectively (Figure 2E). Inhibition of lysosomal degradation by treating animals with chloroquine significantly increased the amount of pro-CPL-1 in WT animals but not in *hlh-30::GFP* animals, suggesting that their lysosomes may be more resistant to inhibition (Figure 2E).

We found that overexpression of HLH-30::GFP had a marginal, slightly positive effect on PTLA in *xbp-1* mutants and did not reverse defective mTORC1 activation following feeding after prolonged L1 arrest (Figures 2F and S2G). As HLH-30 overexpression boosts autophagic capacity of cells via increased lysosome biogenesis/function and autophagosome formation, we tested whether the increased flux through the autophagy pathway prior to lysosomal fusion is compensated for by an increase in lysosome function and whether stimulating lysosome function while restraining autophagy may have added beneficial effects. We found that although *xbp-1* animals overexpressing HLH-30::GFP or harboring a null mutation in *atg-9* were somewhat resistant to PTLA, *xbp-1* animals combining both interventions were remarkably resistant to PTLA, developing after prolonged periods of L1 arrest almost as well as WT animals (Figure 2F). WT animals combining both interventions were also slightly more resistant to PTLA after 9–13 days of L1 arrest (Figure 2F).

Autophagy contributes to lysosome damage and dysfunction in L1-arrested animals

Autophagy clears protein aggregates and P-granules from the cytoplasm during *C. elegans* embryogenesis.[32,35,49] Consistent with previous studies, we found *atg-4.1(bp501)* and *atg-9(bp564)* mutants had 1.5–2 orders of magnitude more SQST-1::GFP puncta than WT animals, mainly localized in the hypodermis (Figures 3A and 3B). SQST-1 is one of five homologs of p62/SQSTM1 encoded in the *C. elegans* genome and is recruited to poly-ubiquitylated protein aggregates in *C. elegans* and promotes their autophagic targeting to lysosomes. Although SQST-1::GFP is cleared by autophagy, the fate of the aggregates that are marked by this protein in lysosomes has not been examined.

Accordingly, we used proteostat dye, which specifically binds to misfolded and aggregated proteins, and a lysosomal membrane marker, SCAV-3::GFP, to test whether protein aggregates are associated with lysosomes in L1-arrested animals.[50–52] In un-arrested L1 animals, SCAV-3::GFP lysosomes were primarily in the pharynx and, to a lesser extent, in the hypodermis, and about ~20% of lysosomes co-localized with aggregates marked by proteostat in WT and *atg-9(bp564)* animals. In arrested animals, SCAV-3::GFP-marked lysosomes were qualitatively more abundant in the hypodermis. In hypodermal cells, protein aggregates were associated with 50%–85% of lysosomes in WT animals during L1 arrest (Figures 3C and 3D). By contrast, the association of protein aggregates with lysosomes was greatly diminished in *atg-9(bp564)* mutants (Figures 3A–3C). These results are reminiscent of the finding that protein aggregates are associated with lysosomes in quiescent neural stem cells, indicating that lysosomal accumulation of protein aggregates is a common feature of quiescent cells.[5]

Lysosomal protein aggregates are commonly associated with lysosome dysfunction. Some studies reported that, via endocytosis, pre-formed fibrils of tau or α-synuclein lead to small perforations in endolysosomal membranes that are repaired by endosomal sorting complex required for transport III (ESCRT-III) machinery.[53,54] Other studies found that pre-formed fibrils of Htt, α-synuclein, and tau(1N3R or 1N4R) lead to endolysosomal rupture and the recruitment of galectins, such as Galectin3, which recruits various machineries to respond to lysosomal membrane disruption.[55–57] In senescent cells, protein aggregates and Galectin3 are associated with lysosomes.[58] Galectins bind to galactoside sugars that are found inside of the lysosomal lumen and can only bind to them when lysosome membranes are damaged.[59] Galectin3, in particular, stabilizes lysosomes from damage and mitigates leakage of lysosomal contents resulting from lysosome-damaging compounds, such as L-leucyl-L-leucine methyl ester (LLOMe).[60] In *C. elegans*, human Galectin3 is recruited to damaged lysosomes in *scav-3* mutants, consistent with its role in responding to and stabilizing lysosome membrane damage.[50]

Accordingly, we created a 3xFLAG::monomeric Azami green (mAG) fusion to human Galectin3 driven by the constitutive promoter *eft-3* and expressed from a single-copy insertion at a safe harbor locus to assess whether lysosomes become damaged during L1 arrest in an autophagy-dependent manner.[61] 3xFLAG::mAG::Galectin3 puncta were rare in un-arrested L1 animals but were recruited to ~1,500 punctate structures in various tissues of *C. elegans*, including the intestine and hypodermis, indicating lysosomal damage (Figures 4A and S3B). Herein, we analyzed 3xFLAG::mAG::Galectin3 localization in the hypodermis, as intestinal cells also contain autofluorescent gut granules at later stages of L1 arrest that make it difficult to distinguish true 3xFLAG::mAG::Galectin3 structures. Co-expression of 3xFLAG::mAG::Galectin3 with the lysosomal luminal protein NUC-1::mCherry (expressed in hypodermal

Please cite this article in press as: Murley et al., Quiescent cell re-entry is limited by macroautophagy-induced lysosomal damage, Cell (2025), https://doi.org/10.1016/j.cell.2025.03.009

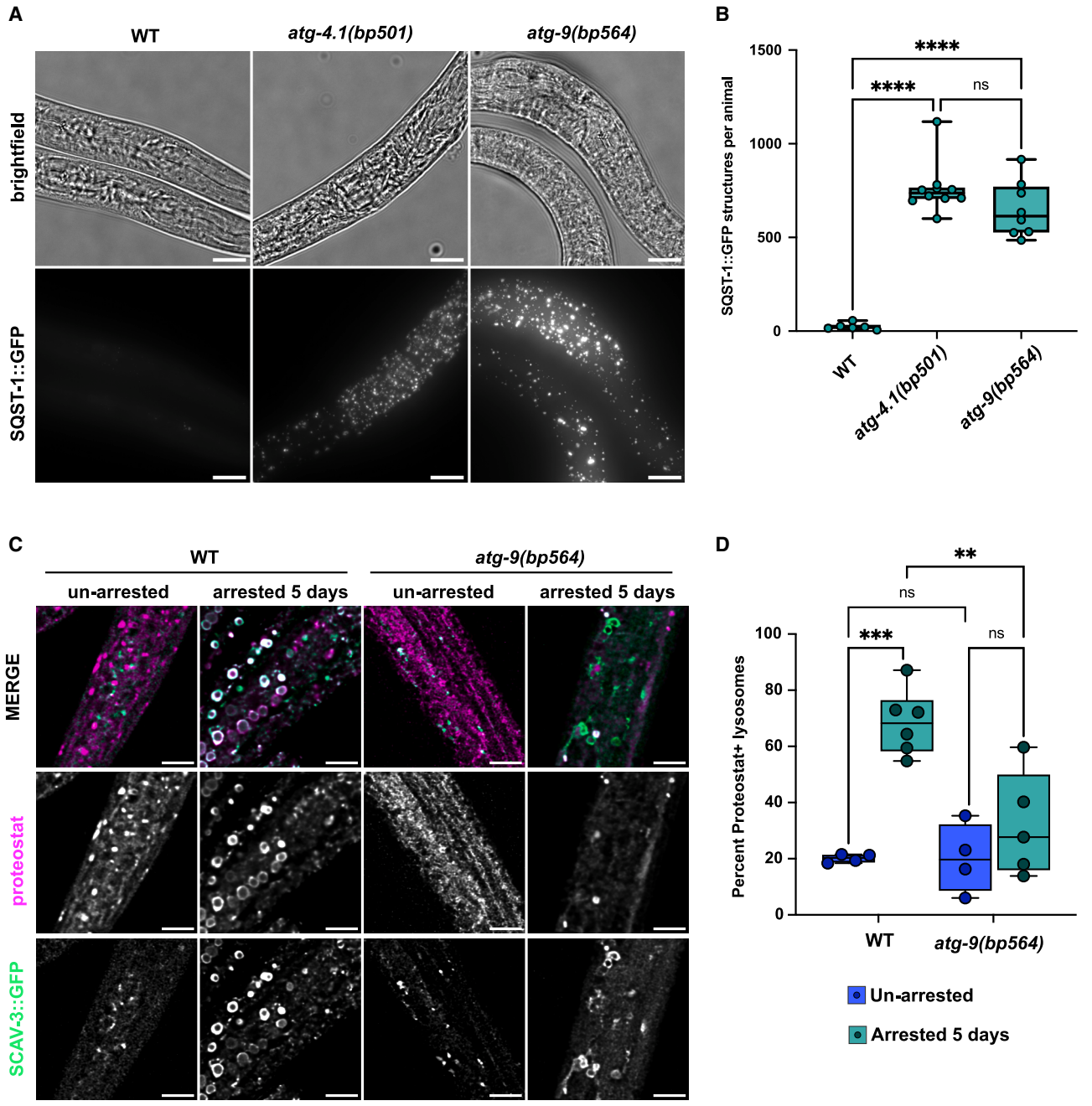

Figure 3. Autophagy results in association of protein aggregates with lysosomes during L1 arrest

(A) Representative images of SQST-1::GFP in arrested L1 animals. Fluorescence images represent a maximum projection image of SQST-1::GFP from entire animals. Bright-field images represent a single focal plane in the center of animals. Scale bars, 10 μm.

(B) Quantification of the number of SQST-1::GFP puncta in WT and *atg-4.1(bp501)* and *atg-9(bp564)* mutant animals L1 arrested for 1 day. *p* values calculated using Tukey's post hoc analysis of a one-way ANOVA (*$p < 0.05$, **$p < 0.01$, ***$p < 0.001$, ****$p < 0.0001$, ns, no significance).

(C) Representative images of proteostat and SCAV-3::GFP-marked lysosomes in hypodermis of WT and *atg-9(bp564)* L1 animals that were never arrested or arrested for 5 days. Scale bars, 5 μm.

(D) Quantification of the percent of SCAV-3::GFP-marked lysosomes in the hypodermis of WT and *atg-9(bp564)* L1 animals that were never arrested or arrested for 5 days. *p* values calculated using Tukey's post hoc analysis of a one-way ANOVA (*$p < 0.05$, **$p < 0.01$, ***$p < 0.001$, ****$p < 0.0001$, ns, no significance).

cells, including the hyp cells, P neuroblasts, and seam cells) revealed that although not all lysosomes are marked by 3xFLAG::mAG::Galectin3, 100% of the puncta formed by 3xFLAG::mAG::Galectin3 associate with lysosomes (Figure 4B).[50,62] Although the recruitment of Galectin3 to lysosomes that retain NUC-1::mCherry seems paradoxical, it is consistent

Please cite this article in press as: Murley et al., Quiescent cell re-entry is limited by macroautophagy-induced lysosomal damage, Cell (2025), https://doi.org/10.1016/j.cell.2025.03.009

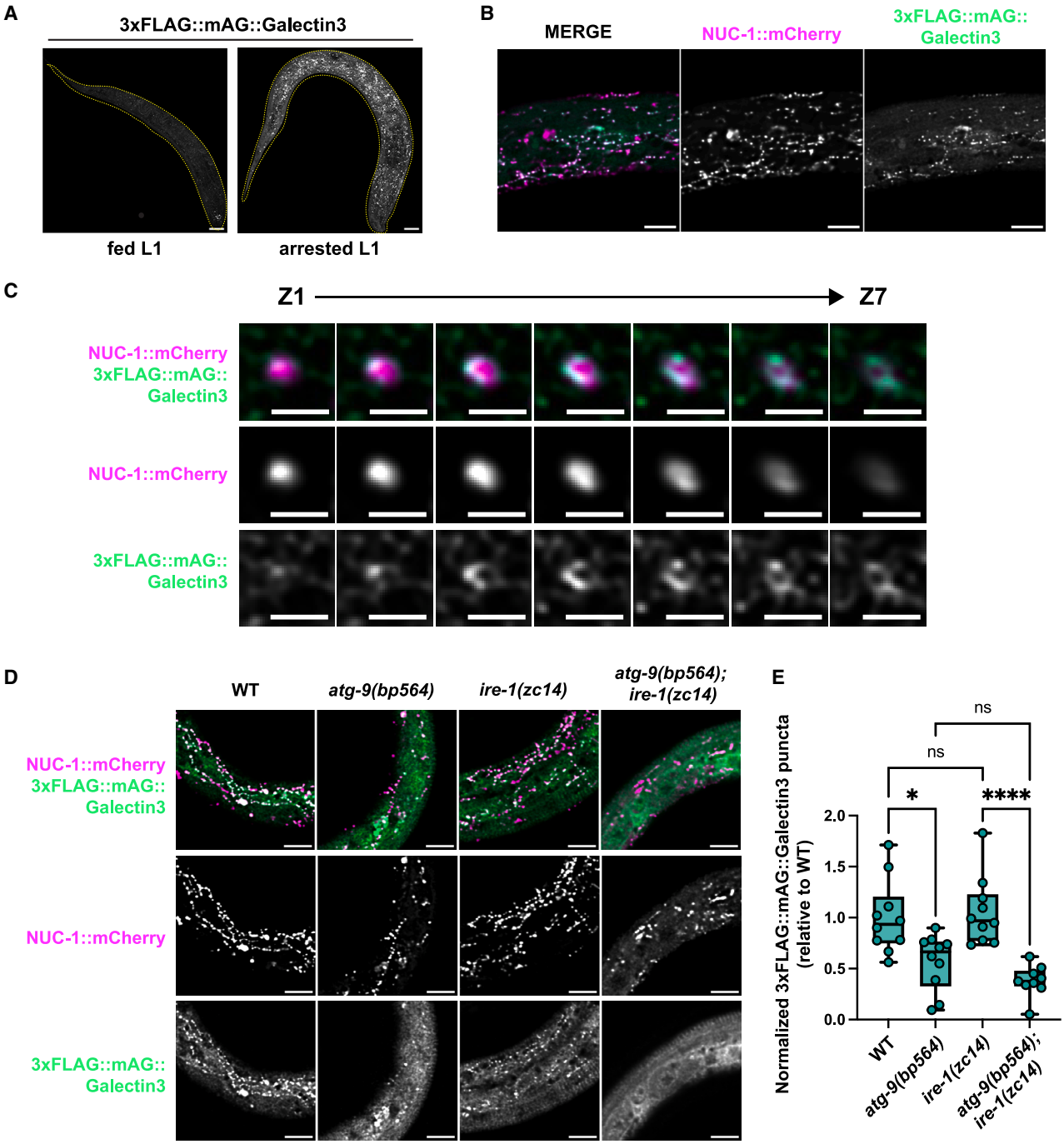

Figure 4. Autophagy contributes to lysosome damage during L1 arrest

(A) Representative maximum projection images of 3xFLAG::mAG::Galectin3 in un-arrested and L1 animals arrested for 2 days, with animal outline in dashed yellow. Scale bars, 10 μm.

(B) 3xFLAG::mAG::Galectin3 puncta are associated with lysosomes in L1-arrested animals. L1 animals arrested for 7 days and expressing 3xFLAG::mAG::-Galectin3 and NUC-1::mCherry (specifically in hypodermal cells) were imaged. A single focal plane is depicted. Scale bars, 5 μm.

(C) A representative Z series (0.15 μm step size) of a NUC-1::mCherry-positive lysosome relative to 3xFLAG::mAG::Galectin3 in hypodermis of L1 animal arrested for 5 days. Scale bar, 1 μm.

(D) Representative micrographs of the hypodermis of WT, *atg-9(bp564)*, *ire-1(zc14)*, and *atg-9(bp564); ire-1(zc14)* animals expressing NUC-1::mCherry and 3xFLAG::mAG::Galectin3. Scale bars, 5 μm.

(legend continued on next page)

Please cite this article in press as: Murley et al., Quiescent cell re-entry is limited by macroautophagy-induced lysosomal damage, Cell (2025), https://doi.org/10.1016/j.cell.2025.03.009

with previous studies indicating that lysosomal proteins are largely retained in lysosomes permeabilized by LLOMe. One study found that molecules greater than 10 kDa are qualitatively retained in lysosomes, which is much smaller than the molecular weight of NUC-1::mCherry, which is approximately 70 kDa, and that of its component parts, which are 43 and 27 kDa, respectively.[63] Furthermore, approximately 70% of lysosomal enzyme activity is retained in lysosomes following LLOMe treatment of human fibroblasts.[64] Super-resolution imaging revealed that 3xFLAG::mAG::Galectin3 was often seen to surround or engulf lysosomes marked by NUC-1::mCherry in hypodermal cells (Figure 4C). As Galectin3 protects lysosomes from damage in mammalian cells, the heterologous expression of 3xFLAG::mAG::Galectin3 might also help to retain lysosomal components in arrested *C. elegans* L1 larvae.[60]

We assessed how autophagy and HLH-30 overexpression influence Galectin3 puncta formation. Consistent with autophagy contributing to lysosomal damage during L1 arrest, fewer 3xFLAG::mAG::Galectin3 puncta were observed in hypodermal cells of *atg-9(bp564)* mutants when normalized to the number of lysosomes marked by NUC-1::mCherry (Figure 4B). As combined autophagy inhibition and HLH-30::GFP overexpression almost completely restore PTLA in *xbp-1* mutants, we tested whether these combined interventions led to a further decrease in lysosome damage (Figure 2F). The 3xFLAG::mAG::Galectin3 reporter formed much brighter and much smaller structures than HLH-30::GFP, which mainly localized to the nucleus in L1-arrested animals, enabling us to confidently identify 3xFLAG::mAG::Galectin3 puncta: in animals expressing only HLH-30::GFP, we only identified ~100 puncta that met the same definition as 3xFLAG::mAG::Galectin3 puncta, which formed ~1,500 puncta in WT animals (Figure S3A). Consistent with HLH-30::GFP overexpression having a marginal effect on PTLA, the numbers of 3xFLAG::mAG::Galectin3 puncta were indistinguishable between WT and HLH-30::GFP-overexpressing animals (Figures S3B and S3C). By contrast, *atg-9(bp564)* mutants overexpressing HLH-30::GFP had far fewer 3xFLAG::mAG::Galectin3 puncta than WT, *hlh-30::GFP*, and *atg-9(bp564)* animals (Figures S3B and S3C). Thus, lysosome damage is well correlated with an inability of *ire-1* and *xbp-1* animals to develop after prolonged L1 arrest (Figures 2F, S3B, and S3C).

Together, the above data indicate that autophagy-dependent accumulation of protein aggregates in lysosomes and corresponding lysosomal damage are correlated with impaired exit from L1 arrest, most especially in *ire-1/xbp-1* mutants. We cannot rule out that defective clearance of protein aggregates from the cytoplasm in *atg* mutants might have negative consequences, but it seems to be a net benefit to the ability of L1-arrested animals to develop after prolonged L1 arrest, especially *ire-1/xbp-1* mutants. Furthermore, although our findings indicate that lysosomal damage and lysosomal accumulation of protein aggregates are a feature of L1-arrested animals, it is unclear which one might cause the other. Lysosomal damage during L1 arrest might prevent the degradation of protein aggregates due to a loss of lysosomal degradative efficiency. Alternatively, as has been reported for certain types of protein aggregates, the aggregates themselves might induce lysosomal membrane damage.[55,57] Consistent with this idea, specifically reducing autophagy of protein aggregates in *sqst-1* mutants—one of five *C. elegans* homologs of SQSTM1/p62 that recruits the autophagy machinery to protein aggregates—mitigated PTLA (Figures S2B and S2C).[49] Regardless, these data indicate that lysosomes are dysfunctional in L1-arrested animals in a way that correlates with the autophagic clearance of protein aggregates from the cytoplasm and their accumulation in lysosomes via autophagy. Inhibiting autophagy and boosting lysosome biogenesis/function work together to mitigate lysosomal damage and dysfunction during L1 arrest.

IRE-1 is required for repair and regeneration of lysosomes following prolonged L1 arrest

Although interventions that reduce lysosome damage correlate with improved recovery from L1 arrest, as shown in Figures 4D and 4E, *ire-1(zc14)* mutants did not have increased 3xFLAG::mAG::Galectin3 puncta compared with WT animals and lysosomal damage precedes PTLA in *ire-1/xbp-1* mutants. This suggests that lysosomal damage per se does not cause permanent cell-cycle arrest. Instead, we hypothesized that IRE-1 and XBP-1 play a role in the response to lysosomal damage that is required to prevent permanent cell-cycle arrest. One possibility is that repair or regeneration of lysosomes requires an optimally functioning ER and unfolded protein response.

To test this, we assessed resolution of lysosomal protein aggregates and lysosomal damage marked by 3xFLAG::mAG::Galectin3. We arrested WT and *ire-1(zc14)* animals expressing 3xFLAG::mAG::Galectin3 and NUC-1::mCherry for 7 days, then fed them for 12 h. In WT animals, there was a dramatic decrease in the number of 3xFLAG::mAG::Galectin3 puncta relative to NUC-1::mCherry lysosomes upon re-feeding. By contrast, there was not a significant reduction in 3xFLAG::mAG::Galectin3 puncta relative to NUC-1::mCherry puncta in *ire-1(zc14)* mutants (Figures 5A and 5B). The association of protein aggregates with lysosomes marked by SCAV-3::GFP was reduced in WT, but not *ire-1(zc14)*, upon re-feeding (Figures 5C and 5D).

Lysosomal proteins are synthesized in the ER, and we hypothesized that *ire-1/xbp-1* may also influence the regeneration of lysosomes following damage during L1 arrest by affecting the biogenesis of lysosomal proteins. To test this idea, we analyzed expression and glycosylation of SCAV-3::GFP by western blotting. Membrane proteins are first glycosylated in the ER, and, consistent with previous studies, we found that SCAV-3::GFP is a glycosylated protein: treatment of extracts from SCAV-3::GFP-expressing animals with peptide N-glycosidase (PNGase) F, which cleaves all glycans, shifted bands migrating at ~130 kDa to bands migrating at ~90 kDa, corresponding to

(E) Quantification and statistical analysis of 3xFLAG::mAG::Galectin3 puncta relative to the number of NUC-1::mCherry (normalized 3xFLAG::mAG::Galectin3 puncta) marked lysosomes in animals of the indicated genotype after 7 days of L1 arrest. *p* values calculated using Tukey's post hoc analysis of a one-way ANOVA (*$p < 0.05$, **$p < 0.01$, ***$p < 0.001$, ****$p < 0.0001$, ns, no significance).
See also Figure S3.

Please cite this article in press as: Murley et al., Quiescent cell re-entry is limited by macroautophagy-induced lysosomal damage, Cell (2025), https://doi.org/10.1016/j.cell.2025.03.009

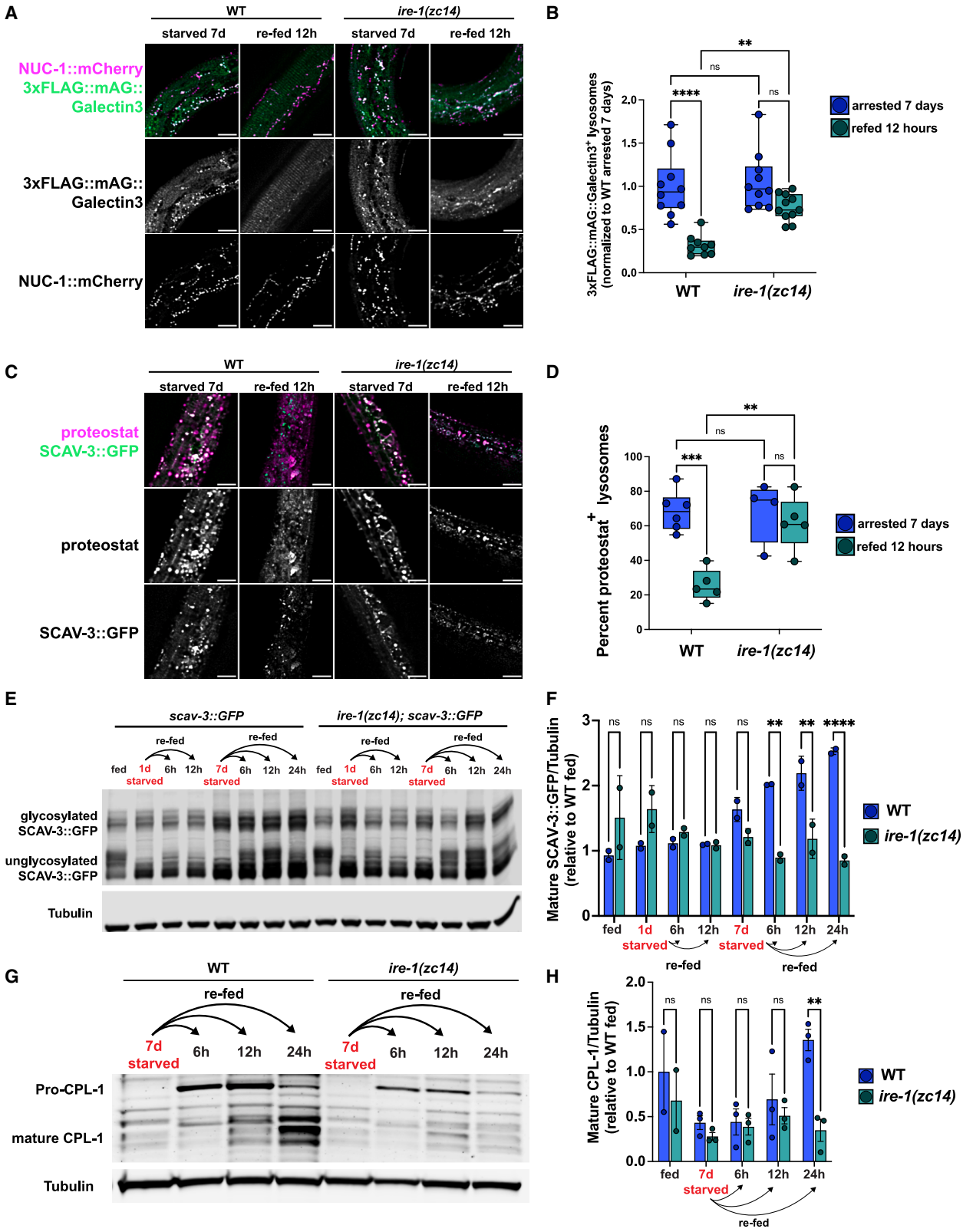

(legend on next page)

Please cite this article in press as: Murley et al., Quiescent cell re-entry is limited by macroautophagy-induced lysosomal damage, Cell (2025), https://doi.org/10.1016/j.cell.2025.03.009

full-length, un-glycosylated SCAV-3::GFP (Figure S4).[50] We also observed a smaller, not previously reported, SCAV-3::GFP isoform approximately ~80 kDa that was sensitive to PNGase F (Figure S4). In un-arrested animals, we observed glycosylated and un-glycosylated SCAV-3::GFP in WT and *ire-1(zc14)* animals. After 1 day of L1 arrest, SCAV-3::GFP was primarily glycosylated and was not significantly affected by 6 or 12 h of feeding, just before animals begin to molt into L2 larvae (Figures 5E and 5F). After 7 days of L1 arrest, levels of glycosylated SCAV-3::GFP were higher than at D1 of arrest and slightly lower in *ire-1(zc14)* mutants. Because animals take longer to develop after prolonged L1 arrest, we analyzed SCAV-3::GFP maturation after 6, 12, and 24 h of feeding, the latter time point being just before WT animals begin to molt into L2 larvae. We found that upon feeding animals following a prolonged 7-day L1 arrest, un-glycosylated SCAV-3::GFP bands began to form, indicating a boost in synthesis of lysosomal proteins, possibly to compensate for lysosome damage (Figures 5E and 5F). Over time, while feeding, glycosylated SCAV-3::GFP levels increased in WT animals but not in *ire-1(zc14)* animals (Figures 5E and 5F). Thus, IRE-1 influences the expression or maturation of lysosomal membrane proteins following prolonged L1 arrest, possibly because of defective protein folding or maturation in the ER.

We also assessed lysosome activity by monitoring the maturation of the cathepsin L protein CPL-1. After 7 days of L1 arrest, CPL-1 expression increased upon feeding, as seen by an increase in pro-CPL-1 that was blunted in *ire-1(zc14)* animals (Figure 5G). Furthermore, levels of mature CPL-1 were lower in *ire-1(zc14)* mutants 24 h after re-feeding following a 7-day L1 arrest, suggesting they are unable to regenerate active lysosomes (Figures 5G and 5H). Notably, the significant reduction in 3xFLAG::mAG::Galectin3 puncta in WT animals fed after 7 days of L1 arrest occurs 12 h after feeding, whereas the formation of significant levels of mature CPL-1 occurs after 24 h of feeding, indicating that resolving lysosome damage marked by 3xFLAG::mAG::Galectin3 is necessary for their reactivation and validates the use of 3xFLAG::mAG::Galectin3 as a marker of lysosome damage/dysfunction (Figures 5A, 5B, 5G, and 5H). Collectively, these findings suggest that the repair, regeneration, and reactivation of lysosomes require IRE-1/XBP-1 and are necessary for cellular rejuvenation and growth following prolonged L1 arrest.

Autophagy causes lysosome damage in quiescent mammalian cells *in vitro*

We tested whether lysosome damage is unique to *C. elegans* L1 arrest because of nutrient deprivation or whether it is a feature of other mitotically quiescent cells. We could robustly induce quiescence in cell culture, using 3T3 Swiss Albino and C3H/10T1/2 mouse fibroblast cells and ARPE-19 human retinal epithelial cells by contact inhibition, while regularly exchanging for fresh media every other day (Figure S5A).[65–67] Levels of the mitotic antigen Ki67 were almost absent in contact-inhibited cells (herein "quiescent") but were restored 48 h after re-plating cells at a lower cell density (Figure S5A).[68] However, over time, the ability to resume proliferation in 3T3 cells was diminished, with a greater proportion of cells having low Ki67 levels 48 h after re-plating, as well as slower growth rates and fewer colonies formed from equivalent numbers of plated viable cells, indicating that an increasing proportion of cells transition from quiescence to irreversible cell-cycle arrest (Figures S5B–S5D).

We tested whether lysosomes harbor increased amounts of protein aggregates in quiescent mammalian cells stably expressing EGFP-Tmem192, which localizes to lysosomal membranes, and stained with proteostat. In all cell lines tested, a greater percentage of lysosomes harbored protein aggregates in quiescent cells than in their proliferating counterparts (Figures 6A–6D).

To assess whether lysosomes become damaged in quiescent mammalian cells, we used Galectin3. mAG-Galectin3 was primarily localized to the cytoplasm and nucleoplasm in proliferating cells but was strikingly recruited to puncta almost exclusively associated with lysosomes marked by Tmem192-mRFP1 in all quiescent cell lines tested (Figures 6E–6H). We also assessed the localization of Galectin3 relative to intact, LysoTracker$^+$ lysosomes in live quiescent cells. We found LysoTracker$^+$ structures were dynamic in cells and that the mAG-Galectin3 recruitment to lysosomes was negatively correlated with LysoTracker staining (Spearman correlation coefficient r_s= -0.56, $p < 0.001$, $n = 155$) (Figures S6A and S6B). Thus, lysosome damage, possibly because of protein aggregates, is a hallmark of quiescent cells.

We used CRISPRi to assess the role of autophagy in lysosomal damage and accumulation of protein aggregates in quiescent

Figure 5. IRE-1 is required for the repair and regeneration of lysosomes following L1 arrest

(A) IRE-1 is required for the resolution of 3xFLAG::mAG::Galectin3 puncta following prolonged L1 arrest. WT and *ire-1(zc14)* animals expressing 3xFLAG::mAG::Galectin3 and NUC-1::mCherry were subjected to arrest for 7 days, then fed for 12 h. Hypodermal cells are depicted. Scale bars, 5 μm.

(B) Quantification and statistical analysis of 3xFLAG::mAG::Galectin3 puncta relative to NUC-1::mCherry puncta in WT and *ire-1(zc14)* animals arrested for 7 days and fed for 12 h. *p* values calculated using Tukey's post hoc analysis of a two-way ANOVA. *$p < 0.05$, **$p < 0.01$, ***$p < 0.001$, ****$p < 0.0001$, ns, no significance.

(C) IRE-1 is required for the reduction in lysosomal protein aggregates in the hypodermis. WT and *ire-1(zc14)* animals expressing SCAV-3::GFP were subjected to L1 arrest for 7 days and fed for 12 h, then fixed, permeabilized, and stained with proteostat as described in STAR Methods. Scale bars, 5 μm.

(D) Quantification and statistical analysis of the percent of lysosomes marked by proteostat in animals of the indicated genotype and conditions. *p* values calculated using Tukey's post hoc analysis of a two-way ANOVA. *$p < 0.05$, **$p < 0.01$, ***$p < 0.001$, ****$p < 0.0001$, ns, no significance.

(E and F) IRE-1 is required for the maturation of SCAV-3::GFP following prolonged L1 arrest. WT and *ire-1(zc14)* animals expressing SCAV-3::GFP were arrested for 7 days, then fed for 6–24 h. A representative western blot is shown in (E), and quantifications of mature SCAV-3::GFP levels (mean ± standard deviation) from two experiments are shown in (F). *p* values were calculated using Tukey's multiple comparison's test of a two-way ANVOA (*$p < 0.05$, **$p < 0.01$, ***$p < 0.001$, ****$p < 0.0001$).

(G and H) IRE-1 is required for the regeneration of mature CPL-1. WT and *ire-1(zc14)* animals were arrested for 7 days, then fed 6–24 h. A representative western blot is shown in (G), and quantification of mature CPL-1 levels (mean ± standard deviation) from three replicates is shown in (H). *p* values were calculated using Tukey's post hoc analysis of a two-way ANOVA. *$p < 0.05$, **$p < 0.01$, ***$p < 0.001$, ****$p < 0.0001$, ns, no significance.

See also Figure S4.

Please cite this article in press as: Murley et al., Quiescent cell re-entry is limited by macroautophagy-induced lysosomal damage, Cell (2025), https://doi.org/10.1016/j.cell.2025.03.009

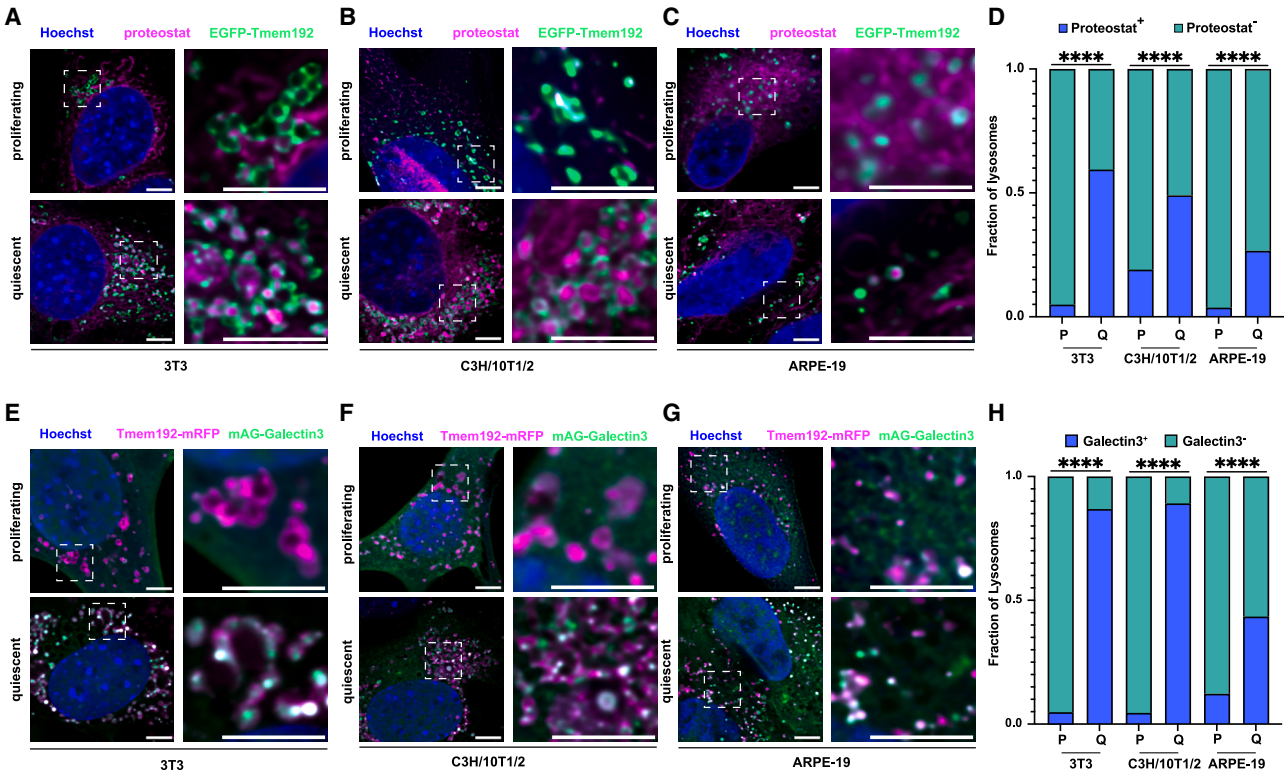

Figure 6. Protein aggregates and Galectin3 are associated with lysosomes in quiescent mammalian cells *in vitro*

(A–C) Intralysosomal protein aggregates accumulate in quiescent mammalian cells. 3T3 Swiss Albino, C3H/10T1/2, and ARPE-19 cells stably expressing EGFP-Tmem192 were grown to confluency and maintained in a contact-inhibited state for 10 days. Quiescent cells and proliferating cells as a control were stained with proteostat to detect protein aggregates side by side and imaged as described in "STAR Methods." Scale bars, 5 μm.

(D) A greater percentage of lysosomes contain protein aggregates in quiescent 3T3 Swiss Albino, C3H/10T1/2, and ARPE-19 cells than their proliferating counterparts. *p* values were calculated using chi-squared test (*$p < 0.05$, **$p < 0.01$, ***$p < 0.001$, ****$p < 0.0001$, ns, no significance).

(E–G) mAG-Galectin3 is recruited to lysosomes in quiescent cells. 3T3-Swiss Albino, C3H/10T1/2, and ARPE-19 cells stably expressing mAG-Galectin3 and Tmem192-mRFP1 were grown to confluency and maintained in a contact-inhibited state for 10 days. Quiescent cells and their proliferating counterparts were fixed, stained with Hoechst, and imaged. Scale bars, 5 μm.

(H) The proportion of lysosomes marked by mAG-Galectin3 in quiescent cells. *p* values were calculated using chi-squared test (*$p < 0.05$, **$p < 0.01$, ***$p < 0.001$, ****$p < 0.0001$, ns, no significance).

See also Figures S5 and S6.

3T3 cells. We used an autophagy flux reporter (mCherry-GFP-LC3B) to assess the potency of our knockdown constructs. Accumulation of mCherry-GFP-LCB in lysosomes via autophagy results in an increase in the relative brightness of mCherry to GFP because the latter is quenched in acidic environments. Using this approach, we confirmed that CRISPRi of *Atg5*, *Atg7*, and *Atg9a*, using two different guide RNAs, inhibited autophagy in response to mTOR inhibition (Figure S7A). To test whether genetic inhibition of autophagy reduces recruitment of Galectin3 to lysosomes, we utilized the weighted Mander's correlation coefficient M1 of Tmem192-mRFP1 from background-subtracted images of cells expressing mAG-Galectin3 and Tmem192-mRFP1 as a quantitative and unbiased measure of the extent to which mAG-Galectin3 is recruited to lysosomes in quiescent cells.[69] Based on this measure, the knockdown of autophagy genes reduced the association of mAG-Galectin3 with lysosomes (Figures 7A and 7B). Autophagy knockdown also reduced the proportion of lysosomes containing protein aggregates (Figures 7C and 7D). Thus, consistent with our findings in *C. elegans*, autophagy contributes to lysosome damage in quiescent mammalian cells, possibly by contributing to the accumulation of protein aggregates within lysosomes.

We also used CRISPRi and a chemical inhibitor of Ire1α, AMG-18 (Kira8) to assess the role of autophagy and the UPR in reactivation of quiescent mammalian cells. As our results in *C. elegans* indicated that Ire1 may function in the reactivation of quiescent cells by promoting lysosome regeneration, we first tested whether it was required for reactivation of quiescent cells. Unfortunately, treatment with AMG-18 prevented reattachment of trypsinized cells and, furthermore, caused a growth defect in proliferating cell cultures, complicating our interpretation (data not shown). We therefore grew 3T3 cells to confluency, then inhibited Ire1α using AMG-18 for 10 days.[70,71] We subsequently split cells and plated 1,000 live cells without AMG-18 and assessed the colonies' formation 1 week later. We found that knockdown of autophagy genes in vehicle control cells did not significantly affect the number of colonies formed from quiescent cells replated after 10 days of arrest (Figure S7B). Treatment of

Please cite this article in press as: Murley et al., Quiescent cell re-entry is limited by macroautophagy-induced lysosomal damage, Cell (2025), https://doi.org/10.1016/j.cell.2025.03.009

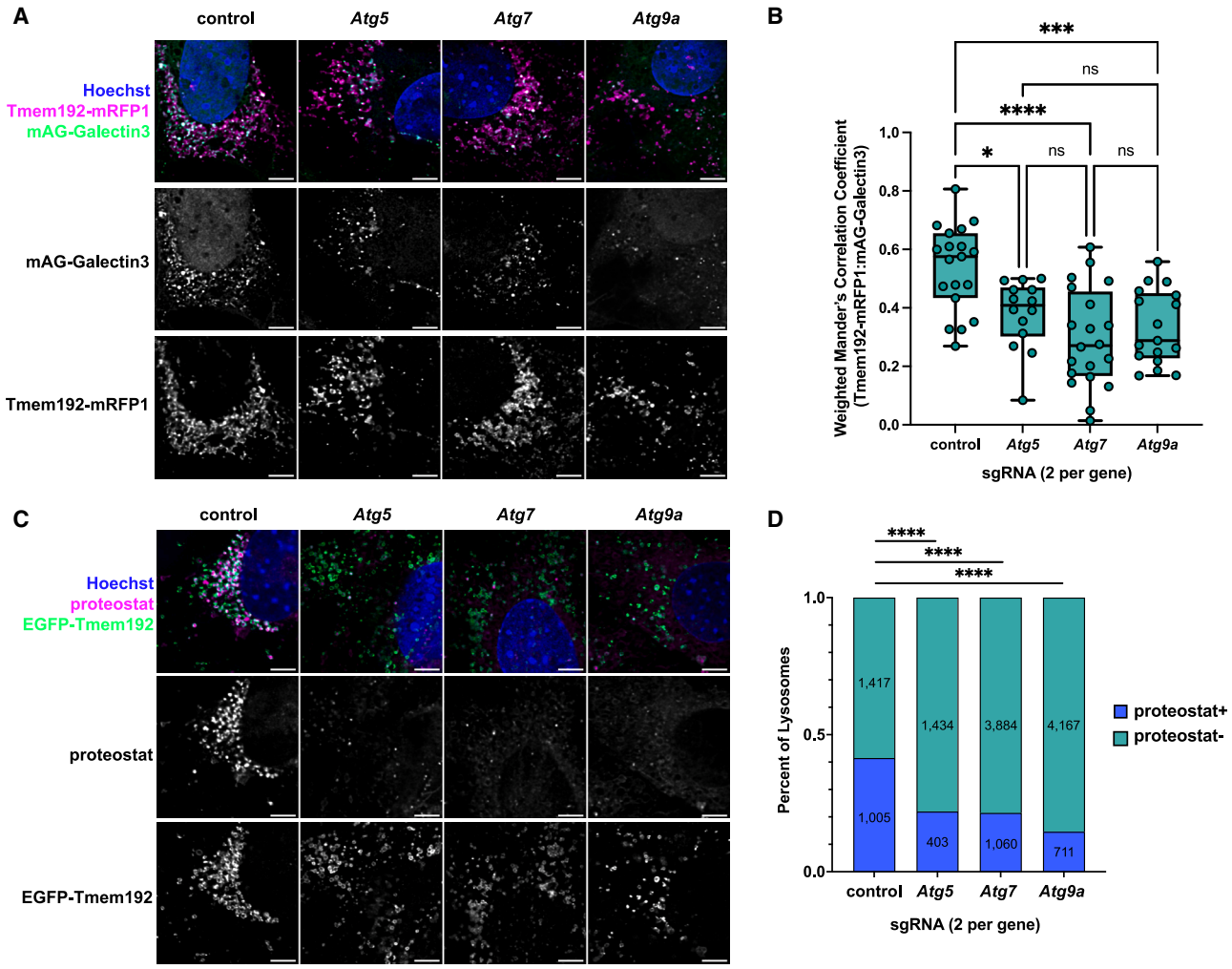

Figure 7. Autophagy contributes to the lysosomal accumulation of protein aggregates and recruitment of Galectin3

(A and B) Autophagy influences lysosomal association of mAG-Galectin3. 3T3-Swiss Albino cells expressing Tmem192-mRFP1, mAG-Galectin3, pHR-UCOE-SFFV-Zim3-dCas9-P2A-Hygro, and non-targeting sgRNA constructs (control) or sgRNA constructs to knock down *Atg5, Atg7*, or *Atg9a* were maintained in a contact-inhibited state for 10 days, fixed, and imaged.

(A) Representative micrographs of contacted inhibited cells of the indicated genotypes. Scale bars, 5 μm.

(B) The weighted Mander's correlation coefficients for Tmem192-mRFP1 relative to mAG-galectin3 from cells in (A) were calculated as described in STAR Methods. *p* values calculated using Tukey's post hoc analysis of a one-way ANOVA (*$p < 0.05$, **$p < 0.01$, ***$p < 0.001$, ****$p < 0.0001$, ns, no significance).

(C and D) Autophagy influences lysosomal accumulation of protein aggregates. 3T3-Swiss Albino cells expressing EGFP-Tmem192, pHR-UCOE-SFFV-Zim3-dCas9-P2A-Hygro, and non-targeting sgRNA constructs (control) or sgRNA constructs to knock down *Atg5*, *Atg7*, or *Atg9a* were maintained in a contact-inhibited state for 10 days, fixed, labeled with proteostat, and imaged. (C) Representative micrographs of contacted inhibited cells of the indicated genotypes. Scale bars, 5 μm. (D) The number of proteostat+ and proteostat- lysosomes from images in (C) were quantified from at least 5 cells per sample. The absolute number of lysosomes in each category is labeled on the bar graphs. *p* values were calculated using chi-squared test (*$p < 0.05$, **$p < 0.01$, ***$p < 0.001$, ****$p < 0.0001$, ns, no significance).

See also Figure S7.

quiescent cells with AMG-18 significantly reduced colony formation, and inhibiting autophagy slightly mitigated the decrease in colonies from AMG-18 treatment (Figure S7B).

DISCUSSION

We have identified a set of processes that contribute to the declining plasticity of quiescent cells. Autophagy in quiescent cells causes lysosome damage, possibly through delivery of protein aggregates that may damage lysosomal membranes. This process can be slowed or reduced in a synergistic manner by inhibiting autophagy and by boosting lysosome biogenesis or function. A degree of cell growth being required for cellular proliferation, reactivation of quiescent cells requires mTORC1 activation, but this is likely inefficient in cells with damaged lysosomes. In *C. elegans*, the unfolded protein response regulators IRE-1/XBP-1 are required for the repair and regeneration of functional lysosomes and development after L1 arrest.

Please cite this article in press as: Murley et al., Quiescent cell re-entry is limited by macroautophagy-induced lysosomal damage, Cell (2025), https://doi.org/10.1016/j.cell.2025.03.009

Autophagy is generally thought to promote longevity by the turnover of dysfunctional and damaging constituents of cells. Consistent with this view are the observations that autophagy is required for the success of all known longevity paradigms in *C. elegans* and that adult-onset perturbation of autophagy causes premature death in mice.[72] Likewise, autophagy flux declines with age, and longevity paradigms tend to mitigate this decline.[5,7,73] Together, these findings suggest that enhanced autophagy may promote longevity. However, our findings suggest that autophagy may also have a detrimental effect on quiescent cells that make important contributions to tissue homeostasis and repair. Possibly through the delivery of protein aggregates to lysosomes, autophagy contributes to increasing lysosomal damage during quiescence, leading to impaired mTORC1 reactivation and likely other effects on cellular homeostasis. Our data indicate that lysosome damage is a feature of quiescent cells that transition toward irreversible growth arrest, both in *C. elegans* and mammalian cells. Our study adds to previously published findings centering lysosomal function between reversible cell-cycle arrest (quiescence) and a transition toward irreversible cell-cycle arrest (senescence).[5,58,74,75] Future studies should examine lysosome damage in quiescent cells *in vivo*.

The accumulation of lysosomal damage in quiescent cells is perplexing, given the numerous means cells utilize to repair, degrade, and replace damaged lysosomes.[59,60,76–79] Most mechanistic studies of lysosomal damage and repair processes have used acute treatments to cause damage to lysosomes in proliferating cells. It may be that proliferative growth cues are required for the repair of damaged lysosomes. Consistent with this view are recent findings reporting constitutive endolysosomal damage in neural cells that increases with age.[80] Lysosome damage in quiescent cells constitutes a paradigm to explore lysosome repair processes and lysosomal stress responses, warranting future study.

Our findings differ in some ways from those of earlier studies studying quiescent adult stem cells *in vivo*. The first found that *Atg7*$^{-/-}$ muscle stem cells have increased rates of cell senescence and was interpreted to indicate that autophagy prevents senescence by removing dysfunctional mitochondria.[6] A recent study has clarified the role of autophagy in hematopoietic stem cells in mice, finding that autophagy is essential for the maintenance of hematopoietic stem cells and their multipotent progeny.[81] Knockout of *Atg5* or *Atg7* in hematopoietic stem cells led to increased amino acid uptake and hyperactivation of mTORC1, and defects in hematopoietic stem cell functions were partially reversed by rapamycin treatment.[81] However, the findings from these studies often rely on cell growth from transplantation experiments and cannot exclude the role of reduced growth rates of autophagy-deficient cells. It may be that reduced cell proliferation rates in *Atg5*$^{-/-}$ and *Atg7*$^{-/-}$ cells might appear as an increased proportion of senescent stem cells and perturbed outgrowth of transplanted cells.[82] Our study tested for an absolute ability to exit quiescence, either in the ability of *C. elegans* to develop following L1 arrest or in the ability of cells to form colonies. These studies also did not explore the role of the UPR, and our findings indicate that the deleterious effects of autophagy-mediated lysosome damage become more apparent in UPR-deficient cells. Although the discrepancies between our results and these studies might simply be explained by different requirements for autophagy-mediated processes in certain cell types or experimental paradigms, alternative explanations might also exist. For example, the Atg8/LC3 lipidation machinery, which includes Atg5 and Atg7, is required for TFEB activation and nuclear translocation following acute lysosomal damage.[83] Although *Atg5* and *Atg7* knockout cells might have less lysosome damage resulting from autophagy, they might also be deficient in Tfeb activation from lysosome damage via other processes. Considering our findings, the role of autophagy and lysosome damage on numerous types of quiescent cells *in vivo* should continue to be examined.

Although our findings indicate that autophagy causes lysosome damage in quiescent cells, given the numerous roles that autophagy plays in cellular and organismal homeostasis and in the maintenance of certain stem cell pools, inhibiting autophagy at the organismal level is certain to be detrimental overall and therefore unlikely to be a good therapeutic strategy to protect quiescent cells in mammals.[81] Indeed, whole-body knockdown of *Atg7* in mice causes death in 30 days.[84] Other processes beyond autophagy contribute to lysosome damage, so lysosome damage would not be completely eliminated by reduced autophagy. Furthermore, damaged lysosomes are removed by autophagic machinery.[76] Our findings point instead to other interventions that might maintain or restore the appropriate reactivation of quiescent cells in age. First, interventions that specifically promote lysosomal function and reduce lysosomal damage in quiescent cells should boost their regenerative potential. Second, the IRE-1/XBP-1 branch of the UPR seems to have a critical role in the repair and regeneration of lysosomes in response to damage, allowing for a robust reactivation of mTORC1 and anabolic cellular growth. Because the UPR becomes dysfunctional with age in some cells and tissues, finding ways to mitigate or bypass this decline may prove useful.[85–88] Finally, direct activation of mTORC1 might be a means of bypassing the perturbed lysosomal homeostasis of quiescent cells to facilitate cell growth and proliferation.[13] Indeed, the small molecule MHY1485, a putative activator of mTORC1 and autophagy inhibitor, was found to improve the regeneration of retinal pigment epithelium following injury in zebrafish.[89]

Lysosomal accumulation of protein aggregates, and accompanying lysosomal damage, is likely to play a role in cellular dysfunction in other types of quiescent cells and in human diseases. Previous studies have found that protein aggregates are associated with lysosomes in quiescent neural stem cells and senescent cells.[5,58,90] Lysosome disruption caused by endocytosis or macropinocytosis of human disease-associated proteinaceous aggregates/fibrils, such as Aβ_{1-42}, tau, and α-synuclein, may also be a means for protein aggregates to spread within tissues.[53–55,91–93] Thus, finding ways to mitigate endolysosomal damage from protein aggregates may prove useful for healthy aging of various cell types and tissues in humans, including in neurodegenerative diseases, where it may both prevent the spread of protein aggregates within the brain and stimulate the regenerative potential of quiescent neural stem cells.[5,91] The striking accumulation of damaged endolysosomes in quiescent cells may be a useful paradigm for future exploration of interventions that increase the resiliency of the endolysosomal

system in quiescent cells and beyond, paving the way toward treatments for age-associated diseases associated with endolysosomal dysfunction.

Limitations of the study

Although our study indicates that lysosome repair via IRE-1/XBP-1 is necessary for exit from quiescence in *C. elegans*, we cannot exclude other roles for IRE-1/XBP-1 nor were we able to examine whether lysosome repair is sufficient for cell-cycle re-entry. We also cannot exclude other effects of lysosome damage, such as leakage of lysosome metabolites, protons, and ions mediating some of the processes identified. Finally, we did not examine these processes in adult stem cells in mammals and cannot exclude the possibility that they have mechanisms to prevent or respond to lysosome damage.

RESOURCE AVAILABILITY

Lead contact

Further information and requests for resources and reagents should be directed to, and will be fulfilled by, the lead contact, Andrew Dillin (dillin@berkeley.edu).

Materials availability

This study generated unique reagents (see "key resources table").

Data and code availability

No original code was used in this study.

ACKNOWLEDGMENTS

We thank the University of California Berkeley cell culture facility for providing cell lines and the Vincent J. Coates Genomics Sequencing Lab for sequencing of *C. elegans* genomic sequences. Graphical abstract created in BioRender, Murley, A. (2025) https://BioRender.com/j45y431. A.M. was supported by a fellowship from the Damon Runyon Cancer Research Foundation, K.W. was supported by a fellowship from the National Science Foundation, and A.D. is an investigator of the Howard Hughes Medical Institute. N.R.G. is an HHMI fellow of the Jane Coffin Childs Memorial Fund.

AUTHOR CONTRIBUTIONS

Conceptualization, A.M. and A.D.; methodology, A.M.; validation, A.M.; formal analysis, A.M.; investigation, A.M., A.C.P., X.S.H., A.L., K.W., E.K., J.D., L.J., H.Z., and N.R.G.; resource provision, A.D.; data curation, A.M., L.J., and A.D.; writing – original draft preparation, A.M.; writing – review & editing, A.M., A.C.P., X.S.H., A.L., K.W., E.K., J.D., L.J., H.Z., N.R.G., and A.D.; visualization preparation, A.M.; supervision, A.D.; project administration, A.M.; funding acquisition, A.M. and A.D.

DECLARATION OF INTERESTS

The authors declare no competing interests.

STAR★METHODS

Detailed methods are provided in the online version of this paper and include the following:

- KEY RESOURCES TABLE
- EXPERIMENTAL MODEL AND STUDY PARTICIPANT DETAILS
  - *C. elegans*
  - Mammalian Cells
- METHOD DETAILS
  - L1 arrest
  - EMS mutagenesis screen
  - Creation of 3xFLAG::mAG::Galectin3 transgenic *C. elegans*
  - Lentivirus production and stable cell line creation
  - Western Blots
  - Fluorescence microscopy
  - Image Analysis
  - Flow Cytometry
  - Autophagy Flux assays in mammalian cells
- QUANTIFICATION AND STATISTICAL ANALYSIS

Received: June 26, 2024
Revised: January 14, 2025
Accepted: March 6, 2025
Published: April 8, 2025

REFERENCES

1. López-Otín, C., Blasco, M.A., Partridge, L., Serrano, M., and Kroemer, G. (2023). Hallmarks of aging: an expanding universe. Cell *186*, 243–278. https://doi.org/10.1016/j.cell.2022.11.001.
2. Marescal, O., and Cheeseman, I.M. (2020). Cellular Mechanisms and Regulation of Quiescence. Dev. Cell *55*, 259–271. https://doi.org/10.1016/j.devcel.2020.09.029.
3. van Velthoven, C.T.J., and Rando, T.A. (2019). Stem Cell Quiescence: Dynamism, Restraint, and Cellular Idling. Cell Stem Cell *24*, 213–225. https://doi.org/10.1016/j.stem.2019.01.001.
4. Kalamakis, G., Brüne, D., Ravichandran, S., Bolz, J., Fan, W., Ziebell, F., Stiehl, T., Catalá-Martinez, F., Kupke, J., Zhao, S., et al. (2019). Quiescence Modulates Stem Cell Maintenance and Regenerative Capacity in the Aging Brain. Cell *176*, 1407–1419.e14. https://doi.org/10.1016/j.cell.2019.01.040.
5. Leeman, D.S., Hebestreit, K., Ruetz, T., Webb, A.E., McKay, A., Pollina, E.A., Dulken, B.W., Zhao, X., Yeo, R.W., Ho, T.T., et al. (2018). Lysosome activation clears aggregates and enhances quiescent neural stem cell activation during aging. Science *359*, 1277–1283. https://doi.org/10.1126/science.aag3048.
6. García-Prat, L., Martínez-Vicente, M., Perdiguero, E., Ortet, L., Rodríguez-Ubreva, J., Rebollo, E., Ruiz-Bonilla, V., Gutarra, S., Ballestar, E., Serrano, A.L., et al. (2016). Autophagy maintains stemness by preventing senescence. Nature *529*, 37–42. https://doi.org/10.1038/nature16187.
7. Zhang, H., Alsaleh, G., Feltham, J., Sun, Y., Napolitano, G., Riffelmacher, T., Charles, P., Frau, L., Hublitz, P., Yu, Z., et al. (2019). Polyamines Control eIF5A Hypusination, TFEB Translation, and Autophagy to Reverse B Cell Senescence. Mol. Cell *76*, 110–125.e9. https://doi.org/10.1016/j.molcel.2019.08.005.
8. Moreno-Jiménez, E.P., Flor-García, M., Terreros-Roncal, J., Rábano, A., Cafini, F., Pallas-Bazarra, N., Ávila, J., and Llorens-Martín, M. (2019). Adult hippocampal neurogenesis is abundant in neurologically healthy subjects and drops sharply in patients with Alzheimer's disease. Nat. Med. *25*, 554–560. https://doi.org/10.1038/s41591-019-0375-9.
9. Baugh, L.R. (2013). To grow or not to grow: Nutritional control of development during Caenorhabditis elegans L1 Arrest at Genetics. Genetics *194*, 539–555. https://doi.org/10.1534/genetics.113.150847.
10. Baugh, L.R., and Sternberg, P.W. (2006). DAF-16/FOXO regulates transcription of cki-1/Cip/Kip and repression of lin-4 during C. elegans L1 arrest. Curr. Biol. *16*, 780–785. https://doi.org/10.1016/j.cub.2006.03.021.
11. Kaplan, R.E.W., Webster, A.K., Chitrakar, R., Dent, J.A., and Baugh, L.R. (2018). Food perception without ingestion leads to metabolic changes and irreversible developmental arrest in C. elegans. BMC Biol. *16*, 112. https://doi.org/10.1186/s12915-018-0579-3.
12. Roux, A.E., Langhans, K., Huynh, W., and Kenyon, C. (2016). Reversible Age-Related Phenotypes Induced during Larval Quiescence in C.

Elegans. Cell Metab. *23*, 1113–1126. https://doi.org/10.1016/j.cmet.2016.05.024.

13. Rodgers, J.T., King, K.Y., Brett, J.O., Cromie, M.J., Charville, G.W., Maguire, K.K., Brunson, C., Mastey, N., Liu, L., Tsai, C.-R., et al. (2014). mTORC1 controls the adaptive transition of quiescent stem cells from G0 to G(Alert). Nature *510*, 393–396. https://doi.org/10.1038/nature13255.
14. Adhikari, D., Zheng, W., Shen, Y., Gorre, N., Hämäläinen, T., Cooney, A.J., Huhtaniemi, I., Lan, Z.-J., and Liu, K. (2010). Tsc/mTORC1 signaling in oocytes governs the quiescence and activation of primordial follicles. Hum. Mol. Genet. *19*, 397–410. https://doi.org/10.1093/hmg/ddp483.
15. Leontieva, O.V., Demidenko, Z.N., and Blagosklonny, M.V. (2014). Contact inhibition and high cell density deactivate the mammalian target of rapamycin pathway, thus suppressing the senescence program. Proc. Natl. Acad. Sci. USA *111*, 8832–8837. https://doi.org/10.1073/pnas.1405723111.
16. Carroll, B., Nelson, G., Rabanal-Ruiz, Y., Kucheryavenko, O., Dunhill-Turner, N.A., Chesterman, C.C., Zahari, Q., Zhang, T., Conduit, S.E., Mitchell, C.A., et al. (2017). Persistent mTORC1 signaling in cell senescence results from defects in amino acid and growth factor sensing. J. Cell Biol. *216*, 1949–1957. https://doi.org/10.1083/jcb.201610113.
17. Frakes, A.E., and Dillin, A. (2017). The UPRER: Sensor and Coordinator of Organismal Homeostasis. Mol. Cell *66*, 761–771. https://doi.org/10.1016/j.molcel.2017.05.031.
18. Martínez, G., Duran-Aniotz, C., Cabral-Miranda, F., Vivar, J.P., and Hetz, C. (2017). Endoplasmic reticulum proteostasis impairment in aging. Aging Cell *16*, 615–623. https://doi.org/10.1111/acel.12599.
19. Walter, P., and Ron, D. (2011). The unfolded protein response: from stress pathway to homeostatic regulation. Science *334*, 1081–1086. https://doi.org/10.1126/science.1209038.
20. Hetz, C., Zhang, K., and Kaufman, R.J. (2020). Mechanisms, regulation and functions of the unfolded protein response. Nat. Rev. Mol. Cell Biol. *21*, 421–438. https://doi.org/10.1038/s41580-020-0250-z.
21. Hetz, C., Axten, J.M., and Patterson, J.B. (2019). Pharmacological targeting of the unfolded protein response for disease intervention. Nat. Chem. Biol. *15*, 764–775. https://doi.org/10.1038/s41589-019-0326-2.
22. Liu, Y., Shao, M., Wu, Y., Yan, C., Jiang, S., Liu, J., Dai, J., Yang, L., Li, J., Jia, W., et al. (2015). Role for the endoplasmic reticulum stress sensor IRE1α in liver regenerative responses. J. Hepatol. *62*, 590–598. https://doi.org/10.1016/j.jhep.2014.10.022.
23. Dong, S., Wang, Q., Kao, Y.-R., Diaz, A., Tasset, I., Kaushik, S., Thiruthuvanathan, V., Zintiridou, A., Nieves, E., Dzieciatkowska, M., et al. (2021). Chaperone-mediated autophagy sustains haematopoietic stem-cell function. Nature *591*, 117–123. https://doi.org/10.1038/s41586-020-03129-z.
24. Chen, J., Ou, Y., Li, Y., Hu, S., Shao, L.-W., and Liu, Y. (2017). Metformin extends C. elegans lifespan through lysosomal pathway. eLife *6*, e31268. https://doi.org/10.7554/eLife.31268.
25. Smith, H.J., Lanjuin, A., Sharma, A., Prabhakar, A., Nowak, E., Stine, P.G., Sehgal, R., Stojanovski, K., Towbin, B.D., and Mair, W.B. (2023). Neuronal mTORC1 inhibition promotes longevity without suppressing anabolic growth and reproduction in C. elegans. PLoS Genet. *19*, e1010938. https://doi.org/10.1371/journal.pgen.1010938.
26. Liu, G.Y., and Sabatini, D.M. (2020). mTOR at the nexus of nutrition, growth, ageing and disease. Nat. Rev. Mol. Cell Biol. *21*, 183–203. https://doi.org/10.1038/s41580-019-0199-y.
27. Yamamoto, H., Zhang, S., and Mizushima, N. (2023). Autophagy genes in biology and disease. Nat. Rev. Genet. *24*, 382–400. https://doi.org/10.1038/s41576-022-00562-w.
28. Olivas, T.J., Wu, Y., Yu, S., Luan, L., Choi, P., Guinn, E.D., Nag, S., De Camilli, P.V., Gupta, K., and Melia, T.J. (2023). ATG9 vesicles comprise the seed membrane of mammalian autophagosomes. J. Cell Biol. *222*, e202208088. https://doi.org/10.1083/jcb.202208088.
29. Sawa-Makarska, J., Baumann, V., Coudevylle, N., von Bülow, S., Nogellova, V., Abert, C., Schuschnig, M., Graef, M., Hummer, G., and Martens, S. (2020). Reconstitution of autophagosome nucleation defines Atg9 vesicles as seeds for membrane formation. Science *369*, eaaz7714. https://doi.org/10.1126/science.aaz7714.
30. Matoba, K., Kotani, T., Tsutsumi, A., Tsuji, T., Mori, T., Noshiro, D., Sugita, Y., Nomura, N., Iwata, S., Ohsumi, Y., et al. (2020). Atg9 is a lipid scramblase that mediates autophagosomal membrane expansion. Nat. Struct. Mol. Biol. *27*, 1185–1193. https://doi.org/10.1038/s41594-020-00518-w.
31. Ghanbarpour, A., Valverde, D.P., Melia, T.J., and Reinisch, K.M. (2021). A model for a partnership of lipid transfer proteins and scramblases in membrane expansion and organelle biogenesis. Proc. Natl. Acad. Sci. USA *118*, e2101562118. https://doi.org/10.1073/pnas.2101562118.
32. Wu, F., Li, Y., Wang, F., Noda, N.N., and Zhang, H. (2012). Differential function of the two Atg4 homologues in the aggrephagy pathway in Caenorhabditis elegans. J. Biol. Chem. *287*, 29457–29467. https://doi.org/10.1074/jbc.M112.365676.
33. Hill, S.E., Kauffman, K.J., Krout, M., Richmond, J.E., Melia, T.J., and Colón-Ramos, D.A. (2019). Maturation and Clearance of Autophagosomes in Neurons Depends on a Specific Cysteine Protease Isoform, ATG-4.2. Dev. Cell *49*, 251–266.e8. https://doi.org/10.1016/j.devcel.2019.02.013.
34. Zhang, H., Chang, J.T., Guo, B., Hansen, M., Jia, K., Kovács, A.L., Kumsta, C., Lapierre, L.R., Legouis, R., Lin, L., et al. (2015). Guidelines for monitoring autophagy in Caenorhabditis elegans. Autophagy *11*, 9–27. https://doi.org/10.1080/15548627.2014.1003478.
35. Tian, Y., Li, Z., Hu, W., Ren, H., Tian, E., Zhao, Y., Lu, Q., Huang, X., and Yang, P. (2010). C . elegans Screen Identifies Autophagy Genes Specific to Multicellular Organisms. Cell *141*, 1042–1055. https://doi.org/10.1016/j.cell.2010.04.034.
36. Subramani, S., and Malhotra, V. (2013). Non-autophagic roles of autophagy-related proteins. EMBO Rep. *14*, 143–151. https://doi.org/10.1038/embor.2012.220.
37. Hibshman, J.D., Leuthner, T.C., Shoben, C., Mello, D.F., Sherwood, D.R., Meyer, J.N., and Baugh, L.R. (2018). Nonselective autophagy reduces mitochondrial content during starvation in Caenorhabditis elegans. Am. J. Physiol. Cell Physiol. *315*, C781–C792. https://doi.org/10.1152/ajpcell.00109.2018.
38. Uma Naresh, N., Kim, S., Shpilka, T., Yang, Q., Du, Y., and Haynes, C.M. (2022). Mitochondrial genome recovery by ATFS-1 is essential for development after starvation. Cell Rep. *41*, 111875. https://doi.org/10.1016/j.celrep.2022.111875.
39. Murley, A., Lackner, L.L., Osman, C., West, M., Voeltz, G.K., Walter, P., and Nunnari, J. (2013). ER-associated mitochondrial division links the distribution of mitochondria and mitochondrial DNA in yeast. eLife *2*, e00422. https://doi.org/10.7554/eLife.00422.
40. Lewis, S.C., Uchiyama, L.F., and Nunnari, J. (2016). ER-mitochondria contacts couple mtDNA synthesis with mitochondrial division in human cells. Science *353*, aaf5549. https://doi.org/10.1126/science.aaf5549.
41. Pickrell, A.M., and Youle, R.J. (2015). The roles of PINK1, parkin, and mitochondrial fidelity in Parkinson's disease. Neuron *85*, 257–273. https://doi.org/10.1016/j.neuron.2014.12.007.
42. Wei, J., Long, L., Yang, K., Guy, C., Shrestha, S., Chen, Z., Wu, C., Vogel, P., Neale, G., Green, D.R., et al. (2016). Autophagy enforces functional integrity of regulatory T cells by coupling environmental cues and metabolic homeostasis. Nat. Immunol. *17*, 277–285. https://doi.org/10.1038/ni.3365.
43. Bialik, S., Dasari, S.K., and Kimchi, A. (2018). Autophagy-dependent cell death–where, how and why a cell eats itself to death. J. Cell Sci. *131*, jcs215152.. https://doi.org/10.1242/jcs.215152.
44. Napolitano, G., and Ballabio, A. (2016). TFEB at a glance. J. Cell Sci. *129*, 2475–2481. https://doi.org/10.1242/jcs.146365.

45. Lapierre, L.R., De Magalhaes Filho, C.D., McQuary, P.R., Chu, C.-C., Visvikis, O., Chang, J.T., Gelino, S., Ong, B., Davis, A.E., Irazoqui, J.E., et al. (2013). The TFEB orthologue HLH-30 regulates autophagy and modulates longevity in Caenorhabditis elegans. Nat. Commun. *4*, 2267. https://doi.org/10.1038/ncomms3267.

46. Springhorn, A., and Hoppe, T. (2019). Western blot analysis of the autophagosomal membrane protein LGG-1/LC3 in Caenorhabditis elegans. Methods Enzymol. *619*, 319–336. https://doi.org/10.1016/bs.mie.2018.12.034.

47. Drobny, A., Prieto Huarcaya, S., Dobert, J., Kluge, A., Bunk, J., Schlothauer, T., and Zunke, F. (2022). The role of lysosomal cathepsins in neurodegeneration: Mechanistic insights, diagnostic potential and therapeutic approaches. Biochim. Biophys. Acta Mol. Cell Res. *1869*, 119243. https://doi.org/10.1016/j.bbamcr.2022.119243.

48. Sun, Y., Li, M., Zhao, D., Li, X., Yang, C., and Wang, X. (2020). Lysosome activity is modulated by multiple longevity pathways and is important for lifespan extension in C. elegans. eLife *9*, e55745. https://doi.org/10.7554/eLife.55745.

49. Lin, L., Yang, P., Huang, X., Zhang, H., Lu, Q., and Zhang, H. (2013). The scaffold protein EPG-7 links cargo-receptor complexes with the autophagic assembly machinery. J. Cell Biol. *201*, 113–129. https://doi.org/10.1083/jcb.201209098.

50. Li, Y., Chen, B., Zou, W., Wang, X., Wu, Y., Zhao, D., Sun, Y., Liu, Y., Chen, L., Miao, L., et al. (2016). The lysosomal membrane protein SCAV-3 maintains lysosome integrity and adult longevity. J. Cell Biol. *215*, 167–185. https://doi.org/10.1083/jcb.201602090.

51. Shen, D., Coleman, J., Chan, E., Nicholson, T.P., Dai, L., Sheppard, P.W., and Patton, W.F. (2011). Novel cell- and tissue-based assays for detecting misfolded and aggregated protein accumulation within aggresomes and inclusion bodies. Cell Biochem. Biophys. *60*, 173–185. https://doi.org/10.1007/s12013-010-9138-4.

52. Navarro, S., and Ventura, S. (2014). Fluorescent dye ProteoStat to detect and discriminate intracellular amyloid-like aggregates in Escherichia coli. Biotechnol. J. *9*, 1259–1266. https://doi.org/10.1002/biot.201400291.

53. Rose, K., Jepson, T., Shukla, S., Maya-Romero, A., Kampmann, M., Xu, K., and Hurley, J.H. (2024). Tau fibrils induce nanoscale membrane damage and nucleate cytosolic tau at lysosomes. Proc. Natl. Acad. Sci. USA *121*, e2315690121. https://doi.org/10.1073/pnas.2315690121.

54. Chen, J.J., Nathaniel, D.L., Raghavan, P., Nelson, M., Tian, R., Tse, E., Hong, J.Y., See, S.K., Mok, S.-A., Hein, M.Y., et al. (2019). Compromised function of the ESCRT pathway promotes endolysosomal escape of tau seeds and propagation of tau aggregation. J. Biol. Chem. *294*, 18952–18966. https://doi.org/10.1074/jbc.RA119.009432.

55. Flavin, W.P., Bousset, L., Green, Z.C., Chu, Y., Skarpathiotis, S., Chaney, M.J., Kordower, J.H., Melki, R., and Campbell, E.M. (2017). Endocytic vesicle rupture is a conserved mechanism of cellular invasion by amyloid proteins. Acta Neuropathol. *134*, 629–653. https://doi.org/10.1007/s00401-017-1722-x.

56. Freeman, D., Cedillos, R., Choyke, S., Lukic, Z., McGuire, K., Marvin, S., Burrage, A.M., Sudholt, S., Rana, A., O'Connor, C., et al. (2013). Alpha-synuclein induces lysosomal rupture and cathepsin dependent reactive oxygen species following endocytosis. PLoS One *8*, e62143. https://doi.org/10.1371/journal.pone.0062143.

57. Kakuda, K., Ikenaka, K., Kuma, A., Doi, J., Aguirre, C., Wang, N., Ajiki, T., Choong, C.-J., Kimura, Y., Badawy, S.M.M., et al. (2024). Lysophagy protects against propagation of α-synuclein aggregation through ruptured lysosomal vesicles. Proc. Natl. Acad. Sci. USA *121*, e2312306120. https://doi.org/10.1073/pnas.2312306120.

58. Johmura, Y., Yamanaka, T., Omori, S., Wang, T.-W., Sugiura, Y., Matsumoto, M., Suzuki, N., Kumamoto, S., Yamaguchi, K., Hatakeyama, S., et al. (2021). Senolysis by glutaminolysis inhibition ameliorates various age-associated disorders. Science *371*, 265–270. https://doi.org/10.1126/science.abb5916.

59. Jia, J., Abudu, Y.P., Claude-Taupin, A., Gu, Y., Kumar, S., Choi, S.W., Peters, R., Mudd, M.H., Allers, L., Salemi, M., et al. (2018). Galectins Control mTOR in Response to Endomembrane Damage. Mol. Cell *70*, 120–135.e8. https://doi.org/10.1016/j.molcel.2018.03.009.

60. Jia, J., Claude-Taupin, A., Gu, Y., Choi, S.W., Peters, R., Bissa, B., Mudd, M.H., Allers, L., Pallikkuth, S., Lidke, K.A., et al. (2020). Galectin-3 Coordinates a Cellular System for Lysosomal Repair and Removal. Dev. Cell *52*, 69–87.e8. https://doi.org/10.1016/j.devcel.2019.10.025.

61. D'Astolfo, D.S., Pagliero, R.J., Pras, A., Karthaus, W.R., Clevers, H., Prasad, V., Lebbink, R.J., Rehmann, H., and Geijsen, N. (2015). Efficient Intracellular Delivery of Native Proteins. Cell *161*, 674–690. https://doi.org/10.1016/j.cell.2015.03.028.

62. Packer, J.S., Zhu, Q., Huynh, C., Sivaramakrishnan, P., Preston, E., Dueck, H., Stefanik, D., Tan, K., Trapnell, C., Kim, J., et al. (2019). A lineage-resolved molecular atlas of C. elegans embryogenesis at single-cell resolution. Science *365*, eaax1971. https://doi.org/10.1126/science.aax1971.

63. Repnik, U., Borg Distefano, M., Speth, M.T., Ng, M.Y.W., Progida, C., Hoflack, B., Gruenberg, J., and Griffiths, G. (2017). L-leucyl-L-leucine methyl ester does not release cysteine cathepsins to the cytosol but inactivates them in transiently permeabilized lysosomes. J. Cell Sci. *130*, 3124–3140. https://doi.org/10.1242/jcs.204529.

64. Eriksson, I., Wäster, P., and Öllinger, K. (2020). Restoration of lysosomal function after damage is accompanied by recycling of lysosomal membrane proteins. Cell Death Dis. *11*, 370. https://doi.org/10.1038/s41419-020-2527-8.

65. Todaro, G.J., and Green, H. (1963). Quantitative studies of the growth of mouse embryo cells in culture and their development into established lines. J. Cell Biol. *17*, 299–313. https://doi.org/10.1083/jcb.17.2.299.

66. Reznikoff, C.A., Brankow, D.W., and Heidelberger, C. (1973). Establishment and characterization of a cloned line of C3H mouse embryo cells sensitive to postconfluence inhibition of division. Cancer Res. *33*, 3231–3238.

67. Dunn, K.C., Aotaki-Keen, A.E., Putkey, F.R., and Hjelmeland, L.M. (1996). ARPE-19, A Human Retinal Pigment Epithelial Cell Line with Differentiated Properties. Exp. Eye Res. *62*, 155–169. https://doi.org/10.1006/exer.1996.0020.

68. Gerdes, J., Lemke, H., Baisch, H., Wacker, H.H., Schwab, U., and Stein, H. (1984). Cell cycle analysis of a cell proliferation-associated human nuclear antigen defined by the monoclonal antibody Ki-67. J. Immunol. *133*, 1710–1715. https://doi.org/10.4049/jimmunol.133.4.1710.

69. Manders, E.M.M., Verbeek, F.J., and Aten, J.A. (1993). Measurement of co-localization of objects in dual-colour confocal images. J. Microsc. *169*, 375–382. https://doi.org/10.1111/j.1365-2818.1993.tb03313.x.

70. Harnoss, J.M., Le Thomas, A., Shemorry, A., Marsters, S.A., Lawrence, D.A., Lu, M., Chen, Y.A., Qing, J., Totpal, K., Kan, D., et al. (2019). Disruption of IRE1α through its kinase domain attenuates multiple myeloma. Proc. Natl. Acad. Sci. USA *116*, 16420–16429. https://doi.org/10.1073/pnas.1906999116.

71. Harrington, P.E., Biswas, K., Malwitz, D., Tasker, A.S., Mohr, C., Andrews, K.L., Dellamaggiore, K., Kendall, R., Beckmann, H., Jaeckel, P., et al. (2015). Unfolded Protein Response in Cancer: IRE1α Inhibition by Selective Kinase Ligands Does Not Impair Tumor Cell Viability. ACS Med. Chem. Lett. *6*, 68–72. https://doi.org/10.1021/ml500315b.

72. Hansen, M., Rubinsztein, D.C., and Walker, D.W. (2018). Autophagy as a promoter of longevity: insights from model organisms. Nat. Rev. Mol. Cell Biol. *19*, 579–593. https://doi.org/10.1038/s41580-018-0033-y.

73. Chang, J.T., Kumsta, C., Hellman, A.B., Adams, L.M., and Hansen, M. (2017). Spatiotemporal regulation of autophagy during Caenorhabditis elegans aging. eLife *6*, e18459. https://doi.org/10.7554/eLife.18459.

74. Fujimaki, K., Li, R., Chen, H., Della Croce, K.D., Zhang, H.H., Xing, J., Bai, F., and Yao, G. (2019). Graded regulation of cellular quiescence depth between proliferation and senescence by a lysosomal dimmer switch.

Proc. Natl. Acad. Sci. USA *116*, 22624–22634. https://doi.org/10.1073/pnas.1915905116.

75. Young, A.R.J., Narita, M., Ferreira, M., Kirschner, K., Sadaie, M., Darot, J.F.J., Tavaré, S., Arakawa, S., Shimizu, S., Watt, F.M., et al. (2009). Autophagy mediates the mitotic senescence transition. Genes Dev. *23*, 798–803. https://doi.org/10.1101/gad.519709.

76. Eapen, V.V., Swarup, S., Hoyer, M.J., Paulo, J.A., and Harper, J.W. (2021). Quantitative proteomics reveals the selectivity of ubiquitin-binding autophagy receptors in the turnover of damaged lysosomes by lysophagy. eLife *10*, e72328. https://doi.org/10.7554/eLife.72328.

77. Zoncu, R., and Perera, R.M. (2022). Built to last: lysosome remodeling and repair in health and disease. Trends Cell Biol. *32*, 597–610. https://doi.org/10.1016/j.tcb.2021.12.009.

78. Radulovic, M., Wenzel, E.M., Gilani, S., Holland, L.K., Lystad, A.H., Phuyal, S., Olkkonen, V.M., Brech, A., Jäättelä, M., Maeda, K., et al. (2022). Cholesterol transfer via endoplasmic reticulum contacts mediates lysosome damage repair. EMBO J. *41*, e112677. https://doi.org/10.15252/embj.2022112677.

79. Tan, J.X., and Finkel, T. (2022). A phosphoinositide signalling pathway mediates rapid lysosomal repair. Nature *609*, 815–821. https://doi.org/10.1038/s41586-022-05164-4.

80. Sanyal, A., Scanavachi, G., Somerville, E., Saminathan, A., Nair, A., Bango Da Cunha Correia, R.F., Aylan, B., Sitarska, E., Oikonomou, A., Hatzakis, N.S., et al. (2025). Neuronal constitutive endolysosomal perforations enable α-synuclein aggregation by internalized PFFs. J. Cell Biol. *224*, e202401136. https://doi.org/10.1083/jcb.202401136.

81. Borsa, M., Obba, S., Richter, F.C., Zhang, H., Riffelmacher, T., Carrelha, J., Alsaleh, G., Jacobsen, S.E.W., and Simon, A.K. (2024). Autophagy preserves hematopoietic stem cells by restraining MTORC1-mediated cellular anabolism. Autophagy *20*, 45–57. https://doi.org/10.1080/15548627.2023.2247310.

82. Tang, A.H., and Rando, T.A. (2014). Induction of autophagy supports the bioenergetic demands of quiescent muscle stem cell activation. EMBO J. *33*, 2782–2797. https://doi.org/10.15252/embj.201488278.

83. Nakamura, S., Shigeyama, S., Minami, S., Shima, T., Akayama, S., Matsuda, T., Esposito, A., Napolitano, G., Kuma, A., Namba-Hamano, T., et al. (2020). LC3 lipidation is essential for TFEB activation during the lysosomal damage response to kidney injury. Nat. Cell Biol. *22*, 1252–1263. https://doi.org/10.1038/s41556-020-00583-9.

84. Mainz, L., Sarhan, M.A.F.E., Roth, S., Sauer, U., Kalogirou, C., Eckstein, M., Gerhard-Hartmann, E., Seibert, H.-D., Voelker, H.-U., Geppert, C., et al. (2022). Acute systemic knockdown of Atg7 is lethal and causes pancreatic destruction in shRNA transgenic mice. Autophagy *18*, 2880–2893. https://doi.org/10.1080/15548627.2022.2052588.

85. Song, J., Ni, Q., Sun, J., Xie, J., Liu, J., Ning, G., Wang, W., and Wang, Q. (2022). Aging Impairs Adaptive Unfolded Protein Response and Drives Beta Cell Dedifferentiation in Humans. J. Clin. Endocrinol. Metab. *107*, 3231–3241. https://doi.org/10.1210/clinem/dgac535.

86. Taylor, R.C., and Dillin, A. (2013). XBP-1 is a cell-nonautonomous regulator of stress resistance and longevity. Cell *153*, 1435–1447. https://doi.org/10.1016/j.cell.2013.05.042.

87. Sabath, N., Levy-Adam, F., Younis, A., Rozales, K., Meller, A., Hadar, S., Soueid-Baumgarten, S., and Shalgi, R. (2020). Cellular proteostasis decline in human senescence. Proc. Natl. Acad. Sci. USA *117*, 31902–31913. https://doi.org/10.1073/pnas.2018138117.

88. Gavilán, M.P., Pintado, C., Gavilán, E., Jiménez, S., Ríos, R.M., Vitorica, J., Castaño, A., and Ruano, D. (2009). Dysfunction of the unfolded protein response increases neurodegeneration in aged rat hippocampus following proteasome inhibition. Aging Cell *8*, 654–665. https://doi.org/10.1111/j.1474-9726.2009.00519.x.

89. Lu, F., Leach, L.L., and Gross, J.M. (2022). mTOR activity is essential for retinal pigment epithelium regeneration in zebrafish. PLoS Genet. *18*, e1009628. https://doi.org/10.1371/journal.pgen.1009628.

90. Curnock, R., Yalci, K., Palmfeldt, J., Jäättelä, M., Liu, B., and Carroll, B. (2023). TFEB-dependent lysosome biogenesis is required for senescence. EMBO J. *42*, e111241. https://doi.org/10.15252/embj.2022111241.

91. Vaquer-Alicea, J., and Diamond, M.I. (2019). Propagation of Protein Aggregation in Neurodegenerative Diseases. Annu. Rev. Biochem. *88*, 785–810. https://doi.org/10.1146/annurev-biochem-061516-045049.

92. Calafate, S., Flavin, W., Verstreken, P., and Moechars, D. (2016). Loss of Bin1 Promotes the Propagation of Tau Pathology. Cell Rep. *17*, 931–940. https://doi.org/10.1016/j.celrep.2016.09.063.

93. Burbidge, K., Rademacher, D.J., Mattick, J., Zack, S., Grillini, A., Bousset, L., Kwon, O., Kubicki, K., Simon, A., Melki, R., et al. (2022). LGALS3 (galectin 3) mediates an unconventional secretion of SNCA/α-synuclein in response to lysosomal membrane damage by the autophagic-lysosomal pathway in human midbrain dopamine neurons. Autophagy *18*, 1020–1048. https://doi.org/10.1080/15548627.2021.1967615.

94. Zhang, Y., Yan, L., Zhou, Z., Yang, P., Tian, E., Zhang, K., Zhao, Y., Li, Z., Song, B., Han, J., et al. (2009). SEPA-1 mediates the specific recognition and degradation of P granule components by autophagy in C. elegans. Cell *136*, 308–321. https://doi.org/10.1016/j.cell.2008.12.022.

95. Galaxy Community (2024). The Galaxy platform for accessible, reproducible, and collaborative data analyses: 2024 update. Nucleic Acids Res. *52*, W83–W94. https://doi.org/10.1093/nar/gkae410.

96. Cantor, J.R., Abu-Remaileh, M., Kanarek, N., Freinkman, E., Gao, X., Louissaint, A., Lewis, C.A., and Sabatini, D.M. (2017). Physiologic Medium Rewires Cellular Metabolism and Reveals Uric Acid as an Endogenous Inhibitor of UMP Synthase. Cell *169*, 258–272.e17. https://doi.org/10.1016/j.cell.2017.03.023.

97. Lehrbach, N.J., Ji, F., and Sadreyev, R. (2017). Next-Generation Sequencing for Identification of EMS-Induced Mutations in Caenorhabditis elegans. Curr. Protoc. Mol. Biol. *117*, 7.29.1–7.29.12. https://doi.org/10.1002/cpmb.27.

98. Frankino, P.A., Siddiqi, T.F., Bolas, T., Bar-Ziv, R., Gildea, H.K., Zhang, H., Higuchi-Sanabria, R., and Dillin, A. (2022). SKN-1 regulates stress resistance downstream of amino catabolism pathways. iScience *25*, 104571. https://doi.org/10.1016/j.isci.2022.104571.

99. Moos, K., Seifert, M., Baumeister, R., and Maier, W. (2014). MiModD. https://mimodd.readthedocs.io/en/latest/.

100. Silva-García, C.G., Lanjuin, A., Heintz, C., Dutta, S., Clark, N.M., and Mair, W.B. (2019). Single-Copy Knock-In Loci for Defined Gene Expression in Caenorhabditis elegans. G3 (Bethesda) *9*, 2195–2198. https://doi.org/10.1534/g3.119.400314.

101. Chen, B., Gilbert, L.A., Cimini, B.A., Schnitzbauer, J., Zhang, W., Li, G.-W., Park, J., Blackburn, E.H., Weissman, J.S., Qi, L.S., et al. (2013). Dynamic imaging of genomic loci in living human cells by an optimized CRISPR/Cas system. Cell *155*, 1479–1491. https://doi.org/10.1016/j.cell.2013.12.001.

102. Sanjana, N.E., Shalem, O., and Zhang, F. (2014). Improved vectors and genome-wide libraries for CRISPR screening. Nat. Methods *11*, 783–784. https://doi.org/10.1038/nmeth.3047.

103. Replogle, J.M., Bonnar, J.L., Pogson, A.N., Liem, C.R., Maier, N.K., Ding, Y., Russell, B.J., Wang, X., Leng, K., Guna, A., et al. (2022). Maximizing CRISPRi efficacy and accessibility with dual-sgRNA libraries and optimal effectors. eLife *11*, e81856. https://doi.org/10.7554/eLife.81856.

104. Wulansari, N., Darsono, W.H.W., Woo, H.J., Chang, M.Y., Kim, J., Bae, E.J., Sun, W., Lee, J.H., Cho, I.J., Shin, H., and Lee, S.J. (2021). Neurodevelopmental defects and neurodegenerative phenotypes in human brain organoids carrying Parkinson's disease-linked DNAJC6 mutations. Sci. Adv. *17*, 7–8. https://doi.org/10.1126/sciadva.abb1540.

Please cite this article in press as: Murley et al., Quiescent cell re-entry is limited by macroautophagy-induced lysosomal damage, Cell (2025), https://doi.org/10.1016/j.cell.2025.03.009

STAR★METHODS

KEY RESOURCES TABLE

REAGENT or RESOURCE	SOURCE	IDENTIFIER
Antibodies		
Anti Phospho-p70S6Kinase (Thr389)	Cell Signaling Technologies	Catalog #9205; RRID: AB_330944
Anti α tubulin	Sigma Aldrich	Catalog #T9026; RRID: AB_477593
Anti Ki67 (SolA5) PE-eFluor610	Thermo Fisher Scientific	Catalog #61-5698-82; RRID: AB_2574620
Anti CPL-1	Origene	Catalog #AP54829PU-N; RRID: AB_11215858
Anti GFP	AMSBIO	Catalog #TP401; RRID: AB_10890443
P44/42 MAPK (Erk1/2) (137F5)	Cell Signaling Technologies	Catalog #4695; RRID: AB_390779
Phospho p44/42 MAPK (Erk1/2) (Thr202/Tyr204) (9101)	Cell Signaling Technologies	Catalog #9101; RRID: AB_331646
Phospho AMPKα (Thr172) (40H9)	Cell Signaling Technologies	Catalog #2535; RRID: AB_331250
Bacterial and virus strains		
E. coli OP50	CGC	OP50, RRID:WB-STRAIN:WBStrain00041969
E. coli OP50::RFP(Kan^R)	This study	N/A
E. coli Stbl3	Thermo Fisher	C7373-03
Chemicals, peptides, and recombinant proteins		
Hoechst	Thermo Fisher Scientific	Catalog# 62249
Torin1	Tocris	Catalog# 4247
Chloroquine diphosphate	Sigma Aldrich	Catalog# C6628-25G
Crystal Violet	Sigma Aldrich	Catalog# 101408
EMS (methanesulfonic acid, ethyl ester)	Sigma Aldrich	Catalog# M-0880
Critical commercial assays		
Proteostat Aggresome Detection Kit	Enzo	Catalog# ENZ-51035-K100
Qubit Protein Broad Range	Thermo Fisher Scientific	Catalog# A50668
Puregene tissue kit	Qiagen	Catalog# 158667
Kapa Biosystems Hyper Prep Kit	Roche	Catalog# KK8504
PNGase F	New England Biolabs	Catalog# P0708S
Lysotracker Red DND-99	Thermo Fisher Scientific	Catalog# L7528
#1.5 glass-like polymer 12 well plates	CellVis	Catalog# P12-1.5P
#1.5 glass-like polymer dishes (35 mm)	CellVis	Catalog# D35-20-1.5P
Human Plasma-Like Medium	Thermo Fisher Scientific	Catalog #A4899102
Experimental models: Cell lines		
3T3-Swiss Albino (*Mus musculus* embryos. Sex unspecified)	University of California Berkeley Cell Culture Core	RRID: CVCL_0120
HEK293T (Female human fetus)	University of California Berkeley Cell Culture Core	RRID: CVCL_0063
C3H/10T1/2 (*Mus musculus* embryos. Sex unspecified)	University of California Berkeley Cell Culture Core	RRID: CVCL_0190
ARPE-19 (Retinal Pigment Epithelium of 19-year-old human male)	University of California Berkeley Cell Culture Core	RRID: CVCL_0145
Experimental models: Organisms/strains		
C. elegans: Wild-type Bristol N2	*Caenorhabditis* Genetics Center	N2; RRID: WB-STRAIN:WBStrain00000001
C. elegans: *ire-1(zc14)II; zcIs4 V*	*Caenorhabditis* Genetics Center	SJ30; RRID:WB-STRAIN:WBStrain00034062
C. elegans: *ire-1(zc14)II* backcrossed 8x to N2	This study	AGD2717
C. elegans: *ire-1(ok799)II*	*Caenorhabditis* Genetics Center	RB925; RRID:WB-STRAIN:WBStrain00031637

(*Continued on next page*)

Please cite this article in press as: Murley et al., Quiescent cell re-entry is limited by macroautophagy-induced lysosomal damage, Cell (2025), https://doi.org/10.1016/j.cell.2025.03.009

Continued

REAGENT or RESOURCE	SOURCE	IDENTIFIER
C. elegans: *ire-1(ok799)II* backcrossed 6x to WT N2	This study	AGD2718
C. elegans: ire-1(ok799)II; atg-4.1 (uth287)I (N156*)	This study	AGD3229
C. elegans: ire-1(ok799)II; atg-9(uth289)V (Q428*)	This study	AGD3231
C. elegans: ire-1(ok799)II; atg-9(uth292)V (Q642*)	This study	AGD3234
C. elegans: ire-1(ok799)II; atg-9(uth346)V (P495S)	This study	AGD4037
C. elegans: ire-1(ok799)II; atg-3(uth347)IV (P205L)	This study	AGD4038
C. elegans: ire-1(ok799)II; atg-18(uth348)V (G26E)	This study	AGD4039
C. elegans: xbp-1(tm2482)*III*	National BioResource Center, Japan	tm2482
C. elegans: xbp-1(tm2482)III tm2482 backcrossed 6x to WT N2	This study	AGD2719
C. elegans: sqIs17[hlh-30p::hlh-30::GFP + rol-6(su1006)]	*Caenorhabditis* Genetics Center	MAH240; RRID:WB-STRAIN: WBStrain00026455
C. elegans: sqIs17[hlh-30p::hlh-30::GFP + rol-6(su1006)] backcrossed 8x to N2	This study	AGD3037
C. elegans: *atg-3(bp412) IV; him-5(e1490) V*	Caenorhabditis Genetics Center	HZ1684; RRID:WB-STRAIN: WBStrain00008597
C. elegans: *ire-1(zc14)II; atg-3(bp412)IV*	This study	AGD3066
C. elegans: *atg-9(bp564)V him-5(e1490) V*	Caenorhabditis Genetics Center	HZ1687; RRID:WB-STRAIN: WBStrain00008600
C. elegans: *atg-9(bp564)V*	This study	AGD3165 (HZ1687 backcrossed 6x to N2)
C. elegans: *ire-1(zc14)II; atg-9(bp564))V*	This study	AGD3309
C. elegans: *xbp-1(tm2482)III; atg-9(bp564)V*	This study	AGD3326
C. elegans: *xbp-1(tm2482)III; sqIs17 [hlh-30p::hlh-30::GFP + rol-6(su1006)]*	This study	AGD2523
C. elegans: *atg-9(bp564)V; sqIs17[hlh-30p::hlh-30::GFP + rol-6(su1006)]*	This study	AGD3374
C. elegans: *xbp-1(tm2482)III; atg-9(bp564)V; sqIs17[hlh-30p::hlh-30::GFP + rol-6(su1006)]*	This study	AGD3327
C. elegans: atg-7(bp422)IV	Hong Zhang, National Institute of Biological Sciences, Beijing, China[94]	AGD2252
C. elegans: ire-1(zc14)II; atg-7(bp422)IV	This study	AGD3068
C. elegans: bpIs151[sqst-1::GFP]IV; him-5	*Caenorhabditis* Genetics Center	HZ589; RRID:WB-STRAIN: WBStrain00008590
C. elegans: bpIs151[sqst-1::GFP]IV	This Study	AGD3214
C. elegans: atg-4.1(bp501)I; bpIs151[sqst-1::GFP]	This Study	AGD3211
C. elegans: bpIs151[sqst-1::GFP]IV; atg-9(bp564)V	This Study	AGD3170
C. elegans: atg-18(gk378)V	*Caenorhabditis* Genetics Center	VC893; RRID:WB-STRAIN: WBStrain00036154
C. elegans: ire-1(zc14)II; atg-18(gk378)V	This study	AGD3071
C. elegans: wbmIs76 IV	*Caenorhabditis* Genetics Center	WBM1179; RRID:WB-STRAIN: WBStrain00040343
C. elegans: wbmIs76[uth322[eft-3p::3xFLAG::mAG::hsLGALS3::unc-54 3'UTR]]	This study	AGD3761
C. elegans: wbmIs76[uth322[eft-3p::3xFLAG::mAG::hsLGALS3::unc-54 3'UTR]]; atg-9(bp564)	This study	AGD3832

(*Continued on next page*)

Please cite this article in press as: Murley et al., Quiescent cell re-entry is limited by macroautophagy-induced lysosomal damage, Cell (2025), https://doi.org/10.1016/j.cell.2025.03.009

Continued

REAGENT or RESOURCE	SOURCE	IDENTIFIER
C. elegans: wbmIs76[uth322[eft-3p::3xFLAG::mAG::hsLGALS3::unc-54 3'UTR]]; atg-9(bp564); sqIs17[hlh-30p::hlh-30::GFP + rol-6(su1006)]	This study	AGD3902
C. elegans: wbmIs76[uth322[eft-3p::3xFLAG::mAG::hsLGALS3::unc-54 3'UTR]]; sqIs17[hlh-30p::hlh-30::GFP + rol-6(su1006)]	This study	AGD3903
unc-76(e911) V; qxIs257[ced-1p::nuc-1::mCherry + unc-76(+)]	*Caenorhabditis* Genetics Center	XW5399; RRID:WB-STRAIN:WBStrain00047716
wbmIs76[uth322[eft-3p::3xFLAG::mAG::hsLGALS3::unc-54 3'UTR]] IV; qxIs257[ced-1p::nuc-1::mCherry + unc-76(+)]	This study	AGD3971
wbmIs76[uth322[eft-3p::3xFLAG::mAG::hsLGALS3::unc-54 3'UTR]]IV; qxIs257[ced-1p::nuc-1::mCherry + unc-76(+)]; ire-1(zc14)II	This study	AGD3972
wbmIs76[uth322[eft-3p::3xFLAG::mAG::hsLGALS3::unc-54 3'UTR]]IV; qxIs257[ced-1p::nuc-1::mCherry + unc-76(+)]; atg-9(bp564)V	This study	AGD3973
wbmIs76[uth322[eft-3p::3xFLAG::mAG::hsLGALS3::unc-54 3'UTR]]IV; qxIs257[ced-1p::nuc-1::mCherry + unc-76(+)];ire-1(zc14)II; atg-9(bp564)V	This study	AGD3974
C. elegans: *qxIs430 [scav-3::GFP + unc-76(+)]*	*Caenorhabditis* Genetics Center	XW5086; RRID:WB-STRAIN:WBStrain00047717
C. elegans: *qxIs430 [scav-3::GFP + unc-76(+)]; ire-1(zc14)II*	This study	AGD3834
C. elegans: *qxIs430 [scav-3::GFP + unc-76(+)]; atg-9(bp564)*	This study	AGD3835
C. elegans: *sqst-1(ok2869)*	*Caenorhabditis* Genetics Center	VC2149; RRID:WB-STRAIN:WBStrain00037114
C. elegans: *sqst-1(ok2869); ire-1(zc14)II*	This study	AGD3221
C. elegans*: pdr-1(gk448)*	*Caenorhabditis* Genetics Center	VC1024; RRID:WB-STRAIN:WBStrain00036256
C. elegans: pdr-1(gk448); ire-1(zc14)II	This study	AGD4048
C. elegans: epg-7(syb4910) X	SUNY Biotechnologies	PHX4910
C. elegans: epg-7(syb4910) X; xbp-1(tm2482) III	This study	AGD3363
Oligonucleotides		
No target #1	CTCGTACTCCGGCAGAGAGC	N/A
No target #2	GAGGTTACCCACCCAGCGGT	N/A
Atg5 #1	GGCACCCGGAGGGATGGCGG	N/A
Atg5 #2	GCAACCCCACCTCCGCCCAG	N/A
Atg7 #1	GTCACAGAATGAGCAACCAG	N/A
Atg7 #2	GTTCCAGACCAGCCCAAAAC	N/A
Atg9a #1	GACGGAGGGCCTAGAGCTCC	N/A
Atg9a #2	GACAGTGAATGACAGACGGA	N/A
Recombinant DNA		
EF1alpha-mAG-Galectin3-Blast	This study	N/A
EF1alpha-Tmem192-mRFP-Neo	This study	N/A
EF1alpha-EGFP-Tmem192-Neo	This study	N/A
pHR-UCOE-SFFV-Zim3-dCas9-P2A-Hygro	Addgene	RRID: Addgene_188768

(*Continued on next page*)

Please cite this article in press as: Murley et al., Quiescent cell re-entry is limited by macroautophagy-induced lysosomal damage, Cell (2025), https://doi.org/10.1016/j.cell.2025.03.009

Continued

REAGENT or RESOURCE	SOURCE	IDENTIFIER
pCDH-EF1a-mCherry-EGFP-LC3B	Addgene	RRID: Addgene_170446
pLENTIGUIDE-FE-Puro	This study	N/A
pMD2.G	Addgene	RRID: Addgene_12259
pMDLg/pRRE	Addgene	RRID: Addgene_12251
pRSV-Rev	Addgene	RRID: Addgene_12253
Software and algorithms		
GraphPad Prism v9.0	Dotmatics	https://www.graphpad.com; RRID: SCR_002798
Adobe Illustrator	Adobe	https://www.adobe.com; RRID: SCR_010279
Adobe Photoshop	Adobe	https://www.adobe.com; RRID: SCR_014199
Fiji	ImageJ	https://imagej.net/software/fiji/; RRID: SCR_002285
Zen Blue (3.1 and 3.3)	Zeiss	https://zeiss.com; RRID: SCR_013672
Galaxy Server	The Galaxy Community[95]	https://usegalaxy.org; RRID: SCR_006281
Image Studio/Image Studio Lite	LI-COR Biotechnology	https://www.licor.com/bio/image-studio-lite/; RRID: SCR_013715

EXPERIMENTAL MODEL AND STUDY PARTICIPANT DETAILS

C. elegans

C. elegans WT Bristol N2 were used as the WT strain background. All mutant strains were backcrossed to N2 at least six times before analysis. Animals were maintained on NGM agar plates seeded with *E. coli* OP50 bacteria.

Mammalian Cells

3T3-Swiss Albino (ATCC CCL-92), C3H/10T1/2 (ATCC CCL-226) and ARPE-19 (ATCC CRL-2302) cells were obtained from the University of California Berkeley cell culture core facility and were free of mycoplasma contamination.[65–67] Cultures remained free of mycoplasma contamination as assessed by periodic Hoechst staining. All cells were grown in Human Plasma-Like Medium (HPLM; Gibco) + 10% Fetal Bovine Serum (FBS) + penicillin/streptomycin in a humidified 37 C incubator in 5% CO_2 and atmospheric O_2 in cell-culture treated plastic dishes (Corning) for routine culturing and growth-based assays or on glass-like polymer dishes (CellVis) for imaging.[96] Media was replaced every other day for proliferating and quiescent cells.

METHOD DETAILS

L1 arrest

Eggs were harvested from well-fed adult hermaphrodites by bleaching. Briefly, animals were washed off plates with M9 buffer, and collected by centrifugation at 1,400 g for 30 seconds in a 15 mL conical tube. Animals were treated with bleaching solution (1.5 % sodium hypochlorite + 645 mM KOH) for about 5 minutes until the adults had broken apart. The eggs were harvested by centrifugation and washed 5x with 15 mL of M9 buffer. Eggs were vortexed for about 1 second and then resuspended in S-basal medium (5.85 g/L NaCl, 1 g/L K_2HPO_4, 6 g/L KH_2PO_4, 5 mg/L cholesterol (from a 5 mg/ml stock in ethanol)) at 5-7 eggs per ul. One day of L1 arrest was defined as 24 hours after bleaching.

To assess animal viability and development, 150-250 animals were spotted directly onto the lawn of OP50 bacteria of 60 mm NGM plates. After 1 hour, animals that had not moved were deemed dead. After 2 days, animals developing to the L3-L4 stage were picked off plates and counted. This was repeated 3 and 4 days after plating and the number of animals removed from plates on days 2-4 was totaled.

EMS mutagenesis screen

Approximately 300 *ire-1(zc14)* or *ire-1(ok799)* L4 larvae were picked into M9 and washed once with M9. Animals were resuspended in M9 buffer with 0.5% of EMS (methanesulfonic acid, ethyl ester, Sigma #M-0880). The tube was nutated at 20 C for 4 hours. After incubation, P0 animals were washed four times with 1mL M9 and allowed to recover on plates. The next day, mutagenized worms that survived EMS treatment were picked onto 10 cm plates with OP50 (10 per plate) and allowed to lay eggs for 48 hours. Three days later, gravid adult F1 animals were bleached and resulting F2 animals were subjected to L1 arrest for 14 days at 20 C. F2 animals were then plated on large OP50 plates, and after 2-4 days at 20 C animals that had developed to the L4 stage were picked singly to OP50 plates at 20 C. Many F2 animals were sterile and were unable to establish lines. Established lines were re-tested for their ability to develop after prolonged L1 arrest.

Please cite this article in press as: Murley et al., Quiescent cell re-entry is limited by macroautophagy-induced lysosomal damage, Cell (2025), https://doi.org/10.1016/j.cell.2025.03.009

Purification of genomic DNA from established suppressor lines was performed using the Puregene Cell and Tissue Kit (Qiagen), as previously described.[97,98] 2ug of purified DNA was sheared using a Covaris S220 focused-ultrasonicator to produce ~400 bp fragments. Library preparation was performed with 1ug of sheared DNA using Kapa Biosystems Hyper Prep Kit (Roche, product number KK8504) with dual index adapters (KAPA, product number KK8727). Sequencing was performed using the Illumina NovaSeq6000 platform through the Vincent J. Coates Genomic Sequencing Core at University of California Berkeley. Raw reads were uploaded to the Galaxy project web platform and the public server was used to analyze the data.[95] Reads were aligned using the Bowtie2 tool with WBcel235/ce11 as the reference genome. The MiModD tool suite was used on the Variant Allele Contrast (VAC) mapping mode to call, extract and filter variants to compare mutants to the parental, un-mutagenized strain.[99]

Creation of 3xFLAG::mAG::Galectin3 transgenic *C. elegans*

Animals expressing the 3xFLAG::mAG::Galectin3 transgene were created using the SKI-LODGE method.[100] Briefly, mAG-Galectin3 was PCR amplified from Addgene plasmid #62734 and purified by ethanol precipitation. The repair template, as well as purified Cas9 ribonucleoprotein complexes with *dpy-10* crRNA were injected into the gonads of D1 adult WBM1179 animals using the SKI-LODGE system as previously described.[100] Lines of fluorescing animals were then genotyped by sequencing analysis to ensure correct insertion of the mAG::Galectin3 transgene, yielding 3xFLAG::mAG::Galectin3.

Lentivirus production and stable cell line creation

Lentiviral vectors were produced in HEK293T cells. One million HEK293T cells were plated per well of a 6 well dish. The following day, 750 ng of equimolar packaging plasmids (pMD2.G, pMDLg/pRRE, pRSV-Rev) and 750 ng of 3rd generation lentiviral transfer plasmids were transfected into cells using lipofectamine P3000. The sequences listed in the "key resources table" were cloned in pLENTIGUIDE F-E, which was modified from lentiguide-PURO with the F-E modification for increased potency used for CRISPRi.[101,102] pHR-UCOE-SFFV-Zim3-dCas9-P2A-Hygro was a gift from Marco Jost & Jonathan Weissman (Addgene plasmid # 188768; http://n2t.net/addgene:188768; RRID:Addgene_188768), mAG-GAL3 was a gift from Niels Geijsen (Addgene plasmid # 62734; http://n2t.net/addgene:62734; RRID:Addgene_62734), pCDH-EF1a-mCherry-EGFP-LC3B was a gift from Sang-Hun Lee (Addgene plasmid # 170446; http://n2t.net/addgene:170446; RRID:Addgene_170446).[61,103,104]

Western Blots

100,000 L1 animals were harvested by centrifugation at 1,400 g for 30 seconds in a 15 mL conical tube and washed twice with M9 buffer. Animals were centrifuged once more without additional M9 to collect residual buffer in the bottom of the tube, which was then aspirated. For Western Blots in Figures 1E, S1B, and S2E, 100 ul of Urea Lysis Buffer (8 M Urea, with 1x NuPage LDS sample buffer + 1% PMSF + 1% phosphatase inhibitor cocktail) was added to animals, which were then transferred to a 1.5 mL microfuge tube and flash frozen in liquid nitrogen and stored at -80C. For all other western blots, RIPA buffer was used with 1% protease inhibitor cocktail and 1% phosphatase inhibitor cocktail. To harvest un-arrested L1 animals, adult animals and larvae were thoroughly washed off of OP50 plates, leaving behind eggs that hatched as L1 larvae harvested by centrifugation as described above 12 hours after adults and larvae were removed from plates. Arrested animals that were subsequently fed were concentrated by centrifugation and spotted onto OP50 plates and harvested by centrifugation 6, 12 or 24 hours later as described above.

Samples in Urea lysis buffer were thawed and sonicated with a probe sonicator (Qsonica Q700) with an amplitude of 10 for seven cycles of two seconds on and one second off. 2-mercaptoethanol was added to a final concentration of 5%. Samples were then heated at 70 C for 10 minutes. Before SDS-PAGE, samples were centrifuged at 17,000 g for 2 minutes.

Samples in RIPA buffer were thawed and sonicated with a probe sonicator (Qsonica Q700) with an amplitude of 10 for seven cycles of two seconds on and one second off. Protein concentrations were determined using the Qubit Protein Broad Range Kit and samples were normalized in RIPA buffer. NuPage LDS Sample buffer and 5% 2-mercaptoethanol were then added and the samples heated to 70 C for 10 minutes. Before SDS-PAGE, samples were centrifuged at 17,000 g for 2 minutes.

For PNGase F treatment, samples were collected in RIPA buffer, flash frozen in liquid nitrogen, thawed, sonicated, and clarified by centrifugation as above. The protein concentrations of clarified lysates were quantitated using the Qubit Protein Broad Range Kit, and 20 total ug of protein was digested with PNGase F (New England Biolabs) according to the manufacturer's instructions. Briefly, denaturation buffer was added to samples at 1X final concentration and then heated to 100 C for 10 minutes. After chilling samples on ice for 3 minutes, Glycobuffer 2 (1X final concentration) and NP-40 (1% final concentration) were added before adding 1000 units of PNGase F. Samples were incubated at 37 C for 2 hours, then NuPage LDS sample buffer and 2-mercaptoethanol (5% final concentration) were added.

Samples were separated on 1.5 mm 4-12% NuPage Bis-Tris gels using 100 V for 2.5 hours, then transferred to 0.45 um nitrocellulose membranes (BioRad Laboratories) for 80 minutes at 100 V. Membranes were blocked in LiCor Intercept TBS blocking buffer for 1 hour at RT, then probed overnight with phosho-S6K(T389) (1:1,000), CPL-1 (1:750), GFP (1:2,000), p44/42 MAPK (1:1,000), phospho-p44/42 MAPK(T202/Y204) (1:1,000), phospho-AMPK(T172) (1:1,000) or alpha tubulin (1:20,000) antibodies at 4 C in LiCor Intercept TBS blocking buffer. Membranes were washed three times for 5 minutes with TBS + 0.05% Tween-20, then probed with appropriate fluorescent secondary antibodies at 1:10,000 for 1 hour in TBS + 0.05% Tween-20, then washed three times for 5 minutes with TBS + 0.05% Tween-20. Membranes were imaged using LiCor Odyssey and band quantification was performed using LiCor Image Studio.

Please cite this article in press as: Murley et al., Quiescent cell re-entry is limited by macroautophagy-induced lysosomal damage, Cell (2025), https://doi.org/10.1016/j.cell.2025.03.009

Fluorescence microscopy

C. elegans L1 larvae were harvested by centrifugation at 1,500 g for 30 seconds and fixed in an equal volume of 4% paraformaldehyde in PBS for 15 minutes at 20-25 C with gentle rotation. Animals were then washed 3x in PBS, sealed under #1.5 coverslips and imaged.

A modified protocol was used to fix/permeabilize worms to stain with proteostat. First, 25,000-50,000 animals were harvested by centrifugation at 1,500 g for 30 seconds in Eppendorf Protein lo-bind tubes. After aspiration of the supernatant, the animals were resuspended in 1 mL of 30% acetone in miliQ water and rotated gently at 20-25 C for 15 minutes in the dark. Animals were washed three times with PBS, then stained with 1:2,000 proteostat in PBS for 2 hours at RT in the dark. Animals were washed three more times with PBS, sealed under #1.5 coverslips and imaged.

Mammalian cells were grown on glass-like polymer dishes (CellVis) to the desired stage, then washed once with PBS, fixed with 4% paraformaldehyde for 15 minutes at RT, then washed 3x with PBS. To stain cells for proteostat, cells were subsequently permeabilized (PBS, 0.2% Tween-20, 2% FBS) for 15 minutes, then washed three times again. Cells were stained with 1:2,000 proteostat in PBS for 2 hours in the dark at RT. Cells were then washed once with gentle rocking for 30 minutes, stained with Hoechst and imaged.

Cells and animals were imaged on an LSM900 Airyscan2 microscope with a 63x 1.4 NA oil immersion objective. Proteostat and mAG/GFP/EGFP tagged proteins were both excited with the 488 nm laser, but to negate bleed-through, fluorophores emitting wavelengths between 490-515 nm and 600-700 nm were used to identify mAG/GFP/EGFP and proteostat, respectively. Three dimensional images were subjected to Airyscan Filtering strength 1.0 and subsequently deconvolved using Zeiss' "Fast Iterative" deconvolution algorithm as part of its Zen 3.1 software.

Image Analysis

Co-localization measurements were performed using Zen 3.3 software. After thresholding to exclude background signal in the two channels, regions of interest were drawn to encompass cells or animals. The correlation coefficients were exported and the median Weighted Mander's correlation coefficient from a Z series through cells was determined.

Quantification of 3xFLAG::mAG::Galectin3 puncta and NUC-1::mCherry lysosomes in *C. elegans* were performed using the "3D Objects Counter" plugin for ImageJ.

Flow Cytometry

Cells were grown to the desired stage of confluency and trypsinized (TrypLE express) for 15 minutes, then quenched with an equal volume of complete growth medium and harvested by centrifugation at 300 g for 4 minutes. Cell pellets were triturated 20 times with a P200 pipette and then fixed/permeabilized with -20 C 90% methanol for 15 minutes. Cells were washed 3x with PBS, then blocked for 30 minutes with 5% normal goat serum for 30 minutes. Fluorescently labeled Ki67 antibody was then added at 1:500 and the cells were probed for 2 hours at RT. Cells were washed 3x with Tris-Buffered Saline with 0.05% Tween-20, then analyzed on an Attune NxT Acoustic Focusing Cytometer.

Autophagy Flux assays in mammalian cells

3T3 Swiss Albino Cells expressing mCherry-EGFP-LC3B, dCas9 and one of two sgRNA constructs against the indicated genes, or targeting no genes as a control, were treated with 100 nM Torin1 or vehicle (DMSO) and imaged every 30 minutes on an IncuCyte (Sartorius) live-cell analysis instrument to collect GFP and mCherry signals.

QUANTIFICATION AND STATISTICAL ANALYSIS

Statistical analyses were performed in GraphPad Prism using tests described in the Figure Legends.

CellPress

Supplemental figures

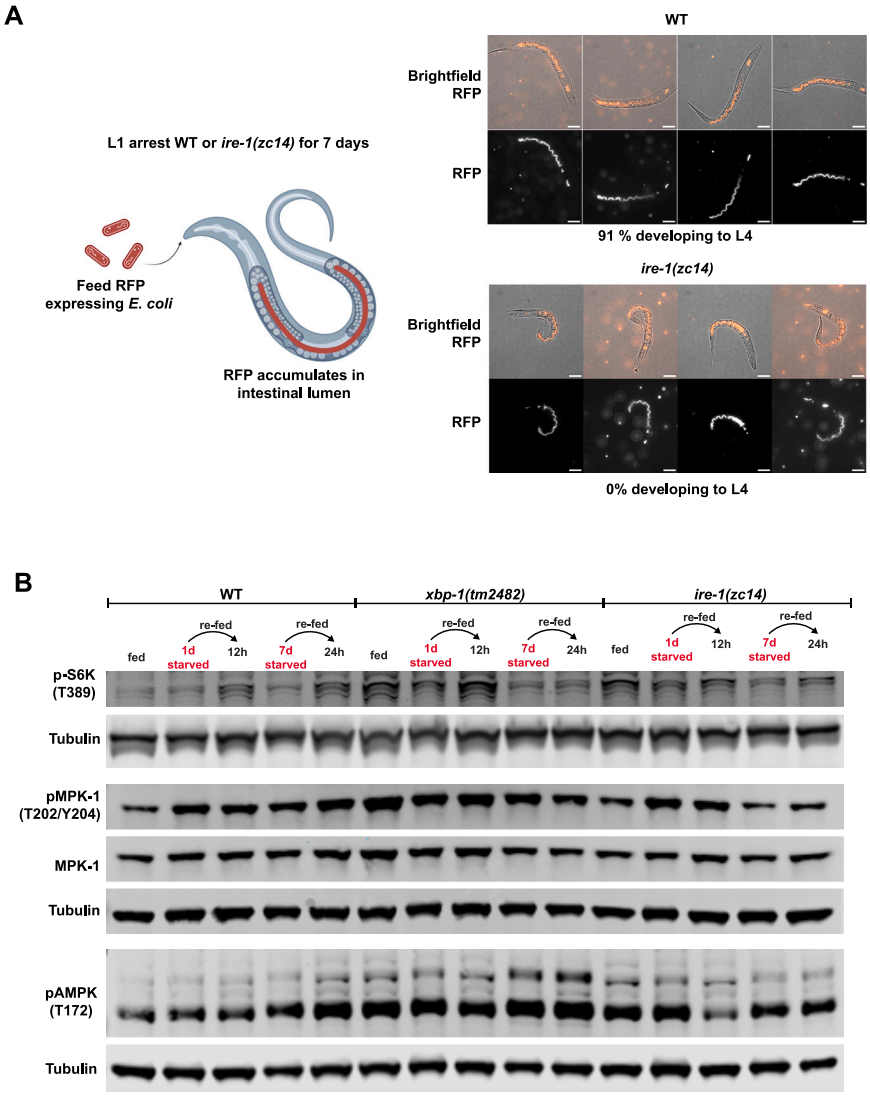

Figure S1. *ire-1* animals can ingest food after prolonged L1 arrest and analysis of mTORC1, AMPK, and mitogen-activated protein kinase (MAPK) signaling during L1 arrest, related to Figure 1

(A) WT and *ire-1(zc14)* L1 animals were arrested for 7 days, then fed *E. coli* OP50 expressing RFP for 8 h and imaged. Animals were also plated on OP50 and scored for their ability to develop to at least the L3 larval stage after 2–4 days. Scale bars, 10 μm.

(B) Un-arrested L1 animals, animals arrested for 1 day and fed for 12 h, and animals arrested for 7 days and fed for 24 h were harvested and subjected to western blot analysis of mTORC1 (pT389S6K), AMPK (pT172), and ERK/MPK-1 (T202/Y204) signaling pathways.

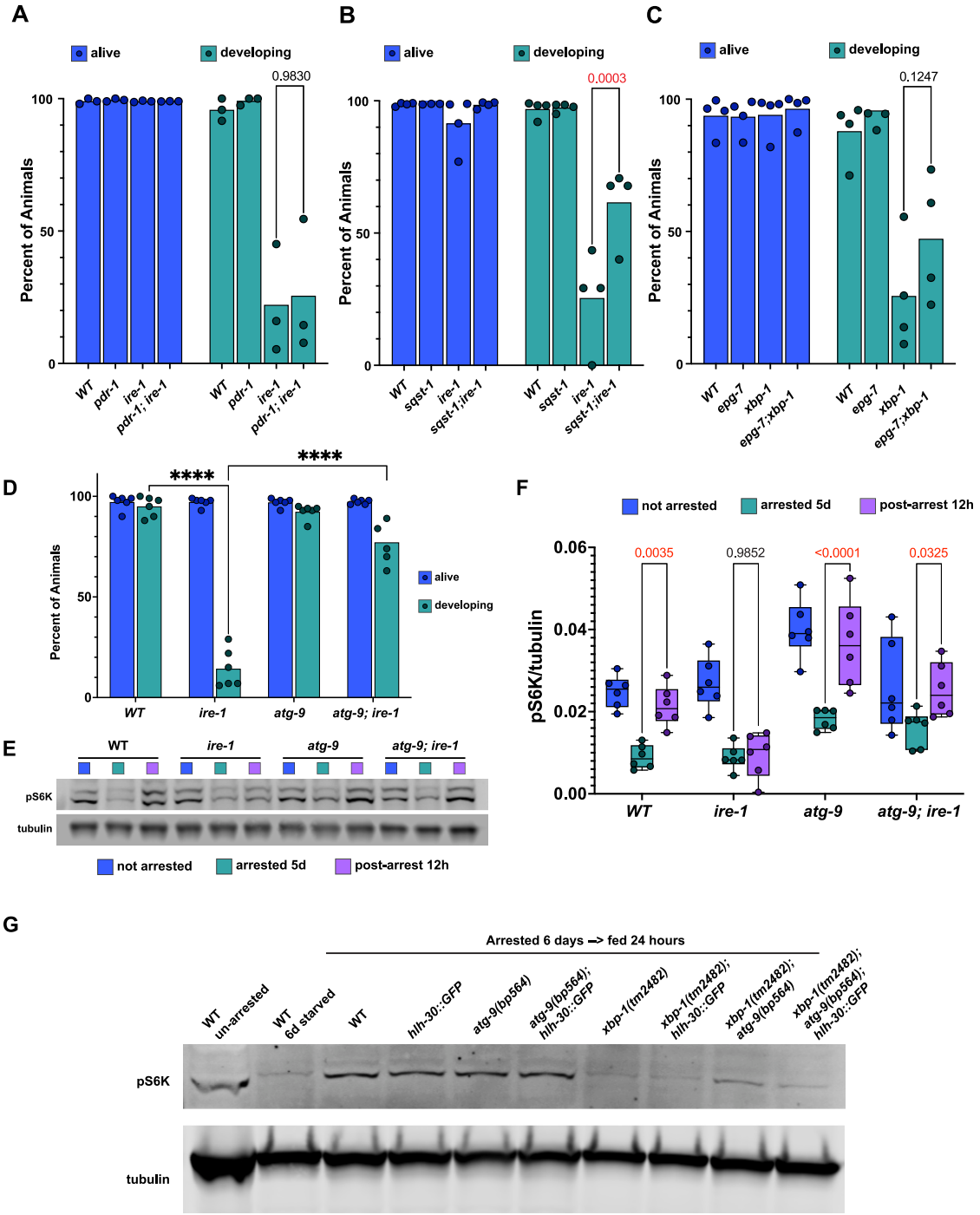

Figure S2. SQST-1, but not PDR-1 or EPG-7, influences PTLA and *atg-9* mutants rescue mTORC1 reactivation in *ire-1(zc14)* animals, related to Figure 2

(A–C) Animals of the indicated genotypes were subjected to a 5-day L1 arrest, then assessed for viability and their ability to develop to at least the L3 larval stage after 2–4 days with food. Each symbol represents an independent biological replicate. *p* values were calculated from an ordinary two-way ANOVA with Tukey's multiple comparisons test. Mutant alleles used were *pdr-1(gk448), sqst-1(ok2869), epg-7(*syb4910), and *ire-1(zc14)*.

(D) *atg-9(bp564)* mutants rescue PTLA in *ire-1(*zc14) mutants. Animals of the indicated genotypes were subjected to a 5-day L1 arrest, then assessed for viability and their ability to develop to at least the L3 larval stage after 2–4 days with food. Each symbol represents an independent biological replicate. *p* values were calculated from an ordinary two-way ANOVA with Tukey's multiple comparisons test (*$p < 0.05$, **$p < 0.01$, ***$p < 0.001$, ****$p < 0.0001$, ns, no significance).

(E) *atg-9(bp564)* rescues mTORC1 reactivation in *ire-1(zc14)* mutants. Animals in (D) were also harvested for western blot analysis of pS6K and tubulin, and a representative western blot is depicted.

(legend continued on next page)

(F) Quantification and statistical analysis of western blots depicted in (E). *p* values calculated using Tukey's post hoc analysis of a one-way ANOVA.
(G) Western blot of pS6K and tubulin from lysates of WT un-arrested L1 animals, WT L1 animals arrested for 6 days, and WT, *hlh-30::GFP*, *atg-9(bp564)*, *atg-9(bp564);hlh-30::GFP*, *xbp-1(tm2482)*, *xbp-1(tm2482);hlh-30::GFP*, *xbp-1(tm2482); atg-9(bp564)*, *and xbp-1(tm2482);hlh-30::GFP;atg-9(bp564)* L1 animals arrested for 6 days and then fed for 24 h.

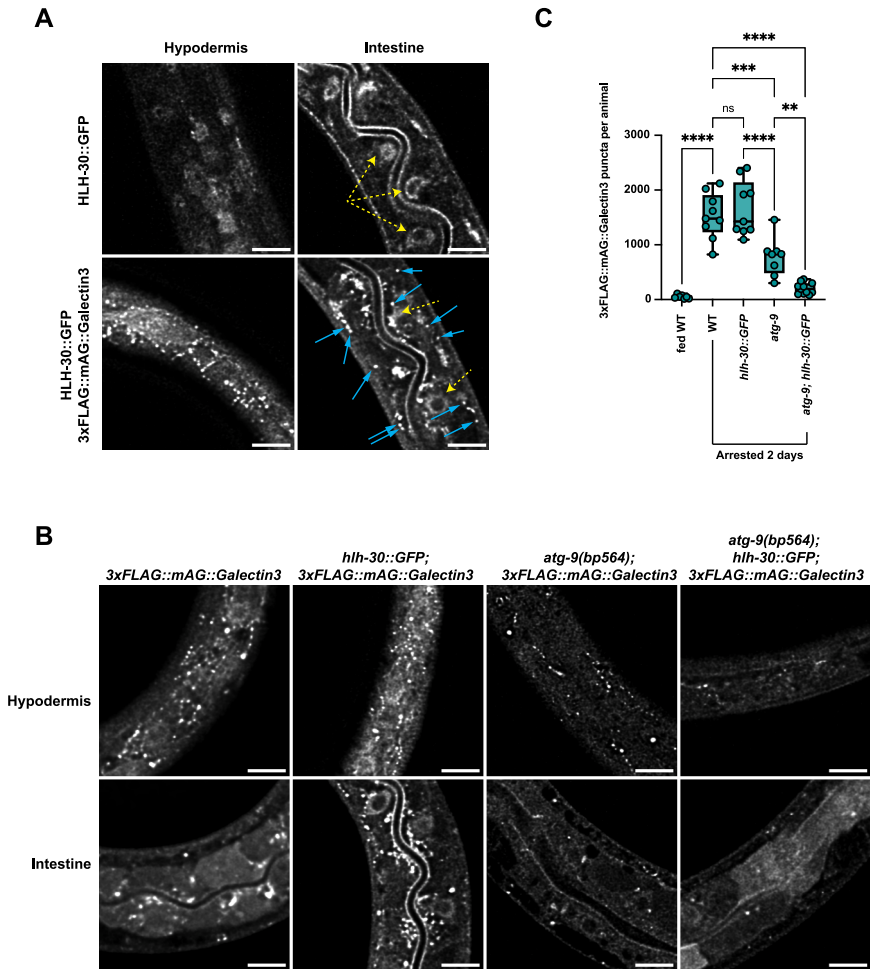

Figure S3. Autophagy inhibition and HLH-30::GFP expression work together to reduce 3xFLAG::mAG::Galectin3 puncta formation, related to Figures 2 and 4

(A) HLH-30::GFP and 3xFLAG::mAG::Galectin3 puncta are distinguishable. Representative micrographs, representing a single focal plane from the hypodermis and intestine, of L1 animals arrested for 2 days expressing HLH-30::GFP alone or HLH-30::GFP and 3xFLAG::mAG::Galectin3. Dashed yellow arrows denote the nucleus (*C. elegans* intestinal cells have large nucleoli), and blue arrows denote 3xFLAG::mAG::Galectin3 puncta. Scale bars, 5 μm.

(B) Representative micrographs of the hypodermis and intestine of L1 animals of the indicated genotypes subjected to L1 arrest for 2 days. Scale bars 5 μm.

(C) Quantification of 3xFLAG::mAG::Galectin3 puncta of animals depicted in (B). *p* values calculated using Tukey's post hoc analysis of a one-way ANOVA (*$p < 0.05$, **$p < 0.01$, ***$p < 0.001$, ****$p < 0.0001$, ns, no significance).

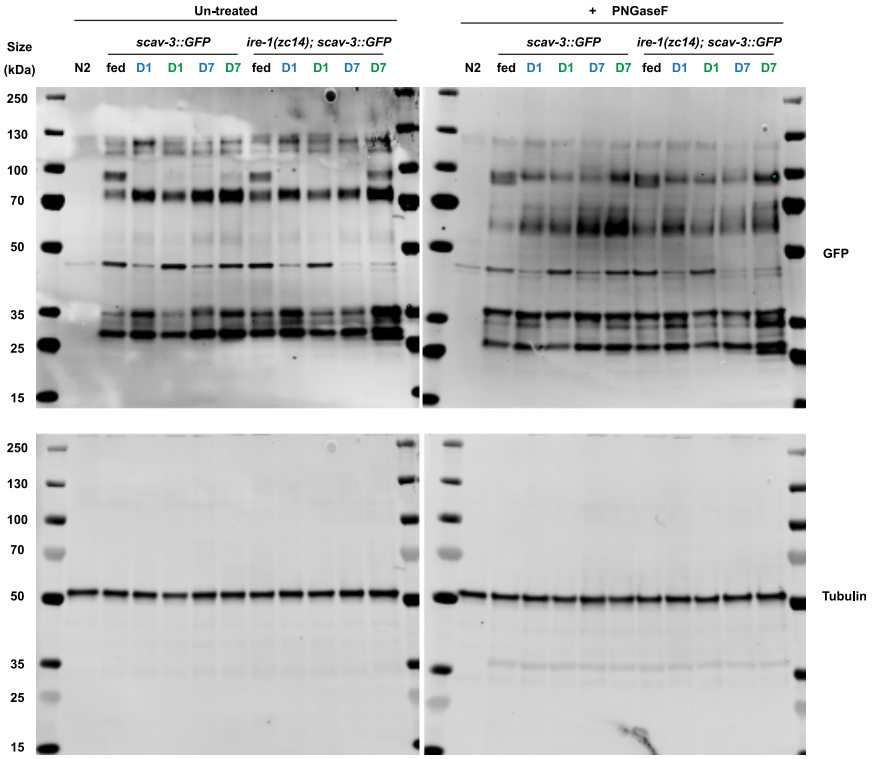

Figure S4. SCAV-3::GFP is a glycosylated protein, related to Figure 5

WT and *ire-1(zc14)* L1 animals expressing SCAV-3::GFP were collected from well-fed plates or were subjected to L1 arrest for 1 day (D1, blue) then re-fed for 12 h (D1, green) or subjected to L1 arrest for 7 days (D7, blue) and re-fed for 12 h (D7, green), lysed in RIPA buffer, and then treated with PNGase F as described in STAR Methods. Treated lysates were subjected to western blot analysis using GFP and tubulin antibodies. WT animals not expressing SCAV-3::GFP (N2) were used as a control for specificity of the GFP antibody. Note the presence of a smaller, previously un-reported SCAV-3::GFP isoform that migrates at about 75–80 kDa that is also sensitive to PNGase F treatment.

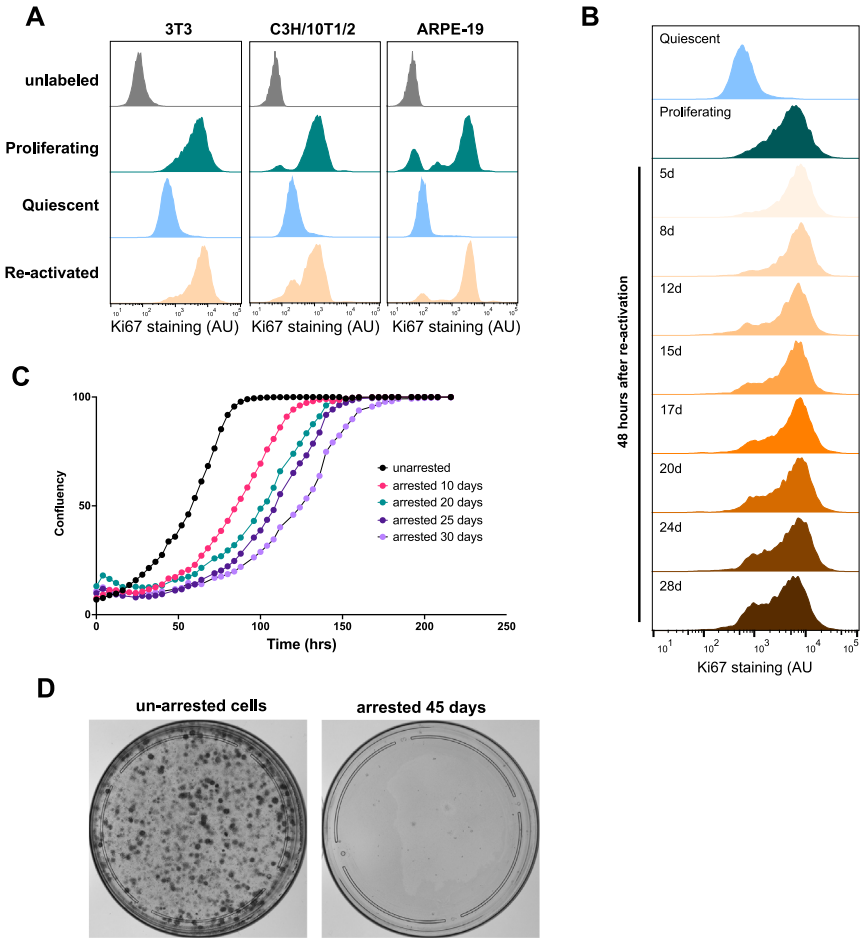

Figure S5. Reversible cell-cycle exit in 3T3 Swiss Albino, C3H10T1/2, and ARPE-19 cells, related to Figure 6

(A) Proliferating cells are cells that were maintained in sub confluent (<70% confluency) for 2 weeks after thawing before harvesting and staining for Ki67 labeling. Quiescent cells were harvested for Ki67 labeling 4 days after reaching confluency. Reactivated cells are quiescent cells that were passaged 1:10 (3T3 and C3H10T1/2) or 1:5 (ARPE-19) and harvested for Ki67 labeling 48 h later. Unlabeled cells are pooled proliferating, quiescent, and reactivated cells that were not stained for Ki67. Cells were labeled with Ki67 antibodies and analyzed by flow cytometry, as described in STAR Methods.

(B) 3T3 Swiss Albino cells were grown to confluency and maintained for the indicated number of days. Cells were split 1:10 and harvested 48 h later, stained for Ki67, and analyzed by flow cytometry.

(C) 3T3 Swiss Albino cells were grown to confluency and maintained for the indicated number of days. They were then split, and 5,000 cells per cm^2 were plated in 6-well plates and imaged on an IncuCyte (Sartorious) and analyzed for confluency every 4 h.

(D) 3T3 Swiss Albino cells were grown to confluency and maintained for 45 days. Cells were passaged alongside a sub-confluent culture, and 1,000 cells were plated on 10-cm dishes and incubated for 7 days until cell colonies formed. Cells were fixed with 4% PFA and stained with crystal violet.

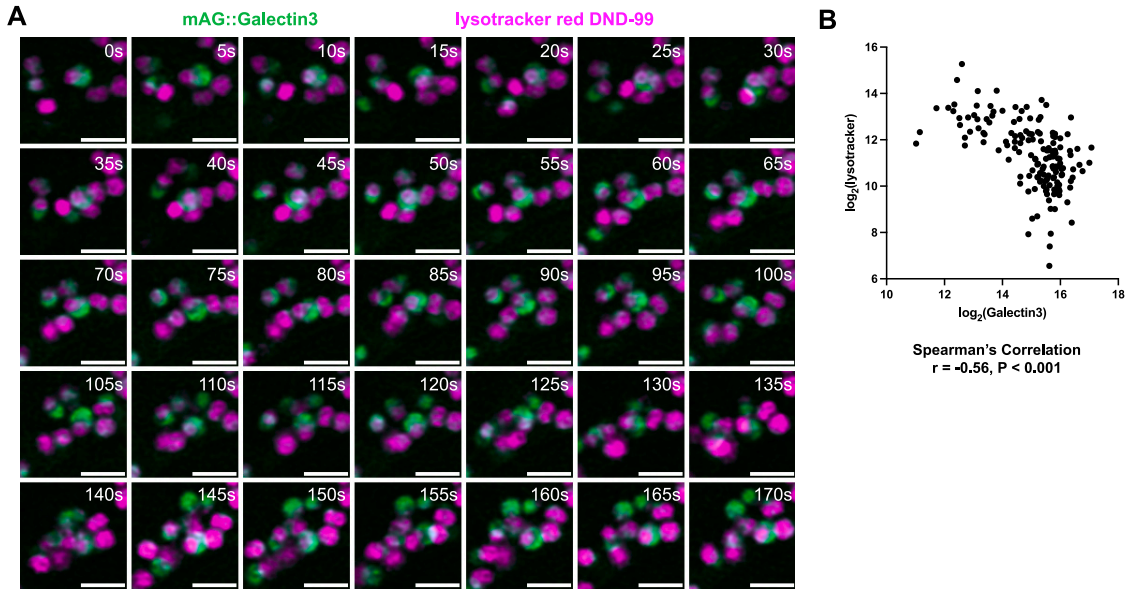

Figure S6. mAG-Galectin3 is negatively correlated with LysoTracker staining of lysosomes in quiescent 3T3 Swiss Albino cells, related to Figure 6

(A) Time-lapse micrographs of 3T3 Swiss Albino cells expressing mAG-Galectin3 and stained with LysoTracker Red DND-99. Scale bars, 2 μm.

(B) LysoTracker staining and mAG-Galectin3 staining are negatively correlated. LysoTracker fluorescence and mAG-Galectin3 fluorescence were measured for 155 LysoTracker+ and/or mAG-Galectin3+ structures in cells, $\log_2$ transformed, and plotted.

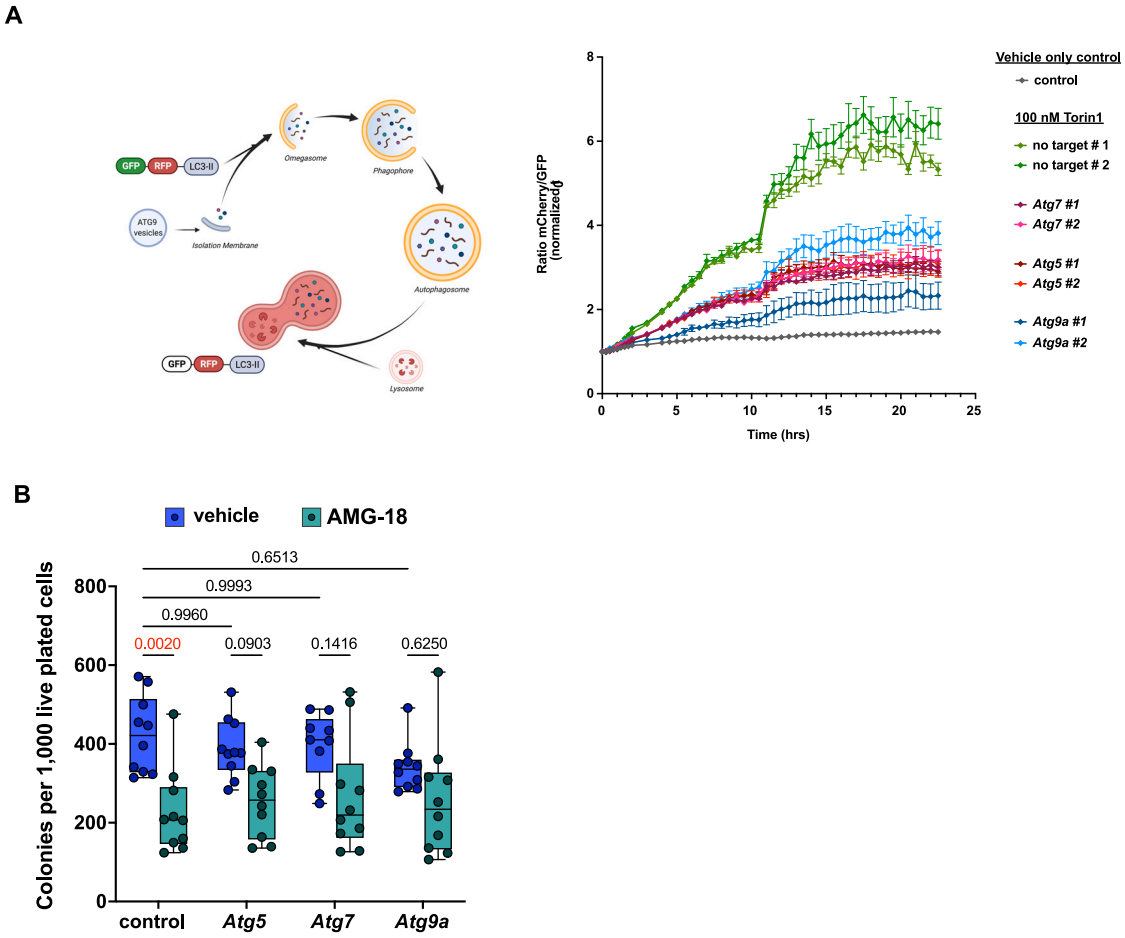

Figure S7. CRISPRi against *Atg5*, *Atg7*, and *Atg9a* reduces autophagy flux and affects cell reactivation, related to Figure 7

(A) Cells expressing mCherry-EGFP-LC3B, dCas9, and one of two sgRNA constructs against the indicated genes, or targeting no genes as a control, were treated with 100 nM Torin1 or vehicle (DMSO) and imaged every 30 min on an IncuCyte live-cell analysis instrument. Vehicle control cells were "no target" control cells. Error bars represent standard deviation.

(B) Cells expressing dCas9 and one of two guide RNA constructs against the indicated genes, no genes as a control, were plated at high cell density (30,000 cells per cm^2) and kept in a confluent, contact-inhibited state for 10 days, exchanging media containing 5 μM AMG-18 or 0.2% DMSO as a vehicle control every other day. The cells were subsequently trypsinized, and 1,000 live cells were plated on 10-cm dishes and allowed to grow into colonies for 1 week.